Ecological Modelling 326 (2016) 124–133

Contents lists available at ScienceDirect

Ecological Modelling

journal homepage: www.elsevier.com/locate/ecolmodel

Lessons learned from applying a forest gap model to understand ecosystem and carbon dynamics of complex tropical forests

Rico Fischer[a,*], Friedrich Bohn[a], Mateus Dantas de Paula[a], Claudia Dislich[b,c], Jürgen Groeneveld[a], Alvaro G. Gutiérrez[d], Martin Kazmierczak[a], Nikolai Knapp[a], Sebastian Lehmann[a], Sebastian Paulick[a], Sandro Pütz[a,e], Edna Rödig[a,f], Franziska Taubert[a], Peter Köhler[g], Andreas Huth[a,h,i]

[a] Helmholtz Centre for Environmental Research GmbH–UFZ, Department of Ecological Modeling, Permoserstr. 15, 04318 Leipzig, Germany
[b] University of Göttingen, Department of Ecosystem Modelling, Büsgenweg 4, 37077 Göttingen, Germany
[c] Helmholtz Interdisciplinary Graduate School of Environmental Research, Helmholtz Centre for Environmental Research—UFZ, Permoserstr. 15, 04318 Leipzig, Germany
[d] Department of Environmental Sciences and Renewable Natural Resources Faculty of Agronomic Sciences, University of Chile, Av. Santa Rosa 11315, La Pintana 8820808, Santiago, Chile
[e] Helmholtz Centre for Environmental Research GmbH–UFZ, Department of Bioenergy, Permoserstr. 15, 04318 Leipzig, Germany
[f] Helmholtz Centre for Environmental Research GmbH–UFZ, Department Computational Hydrosystems, Permoserstr. 15, 04318 Leipzig, Germany
[g] Alfred-Wegener-Institut Helmholtz-Zentrum für Polar- und Meeresforschung (AWI), Am Handelshafen 12, 27570 Bremerhaven, Germany
[h] University of Osnabrück, Institute of Environmental Systems Research, Barbarastr. 12, 49076 Osnabrück, Germany
[i] German Centre for Integrative Biodiversity Research (iDiv) Halle-Jena-Leipzig, Deutscher Platz 5e, 04103 Leipzig, Germany

ARTICLE INFO

Article history:
Received 8 December 2014
Received in revised form
12 November 2015
Accepted 19 November 2015
Available online 4 January 2016

Keywords:
FORMIND
Forest simulations
Species richness
Disturbance
Carbon balance
Structural realism

ABSTRACT

Forests worldwide are threatened by various environmental and anthropogenic hazards, especially tropical forests. Knowledge on the impacts of these hazards on forest structure and dynamics has been compiled in empirical studies. However, the results of these studies are often not sufficient for long-term projections and extrapolations to large spatial scales especially for unprecedented environmental conditions, which require both the identification and understanding of key underlying processes. Forest models bridge this gap by incorporating multiple ecological processes in a dynamic framework (i.e. including a realistic model structure) and addressing the complexity of forest ecosystems. Here, we describe the evolution of the individual-based and process-based forest gap model FORMIND and its application to tropical forests. At its core, the model includes physiological processes on tree level (photosynthesis, respiration, tree growth, mortality, regeneration, competition). During the past two decades, FORMIND has been used to address various scientific questions arising from different forest types by continuously extending the model structure. The model applications thus provided understanding in three main aspects: (1) the grouping of single tree species into plant functional types is a successful approach to reduce complexity in vegetation models, (2) structural realism was necessary to analyze impacts of natural and anthropogenic disturbances such as logging, fragmentation, or drought, and (3) complex ecological processes such as carbon fluxes in tropical forests – starting from the individual tree level up to the entire forest ecosystem – can be explored as a function of forest structure, species composition and disturbance regime. Overall, this review shows how the evolution of long-term modelling projects not only provides scientific understanding of forest ecosystems, but also provides benefits for ecological theory and empirical study design.

1. Introduction

Approximately 25% of Earth's land surface is covered by forests that harbor more than 70% of all terrestrial species (Gibson et al., 2011; Myers et al., 2000; Pimm et al., 2014). Forests contain a huge amount of terrestrial biomass and are therefore an important part of the terrestrial carbon cycle (Grace et al., 2014; Bonan, 2008).

One important factor affecting forest ecosystems is land use. In particular, deforestation poses a major threat to forest ecosystems. Between 2000 and 2012, a loss of 12 million hectares of forest per year was observed, the majority (32%) in tropical forests (Hansen et al., 2013). Degradation of forests caused by tree harvesting

* Corresponding author. Tel.: +49 3412351896; fax: +49 341235451896.
E-mail address: rico.fischer@ufz.de (R. Fischer).

http://dx.doi.org/10.1016/j.ecolmodel.2015.11.018

(Ticktin, 2004), fragmentation (Laurance et al., 2011) as well as climate change (IPCC, 2013) pose additional risks to forests worldwide. Forest loss and degradation result in additional carbon emissions being responsible for about 10% of all anthropogenic carbon emissions (Le Quéré et al., 2015; IPCC, 2013). These processes are also the main drivers of species extinctions (Ceballos et al., 2015). Impacts of disturbances and climate change have been investigated in various field studies (e.g., Debinski and Holt, 2000; Lawton et al., 1998; Anderson-Teixeira et al., 2015). However, to project forest development in the future and to better understand the impacts of multiple anthropogenic threats, ecological models are important tools (Shugart, 2003).

Forest models have a long tradition in ecology and forestry. Starting from simple forest-yield tables in 1787 (Moser, 1980), the incorporation of mathematical equations (representing multiple interacting ecological processes) led in the 1970s to novel types of simulation models, including forest gap models (Botkin et al., 1972) and finally to the development of individual tree-based models (Huston et al., 1988). This development was possible due to the increasing availability of computers.

Gap models have been used to understand forest succession and to investigate the mechanisms underlying the long-term dynamics of forest ecosystems (Bugmann, 2001; Shugart, 1998, 2003; Botkin et al., 1972; Pretzsch, 2009). Initially, forest gap models were applied to temperate forests (Botkin et al., 1972; Bugmann, 2001; Shugart, 1984). For more complex forests found in the tropics, gap models need to account for higher species-richness than in temperate regions. Additionally, unmanaged forests normally consist of patches in different successional stages. Their dynamics are mainly governed by the disturbance events of falling trees creating gaps. Moreover, human-induced disturbances (e.g., logging or fragmentation) affect the overall dynamics of forests in many regions of the world. To include these processes, gap models needed to comprise complexity and structural realism with efficient computing.

Here, we summarize the main achievements of applying the forest gap model FORMIND to complex tropical forests with high species richness, heterogenic structure and dense vegetation. This review addresses the following questions:

(1) How can several hundred different tree species be included in simulations for model applications in species-rich forests?
(2) How can the effect of natural and anthropogenic disturbances on forest structure and forest dynamics be simulated?
(3) How can forest gap models help to project and assess the carbon balance of forests?

2. Developing a forest gap model for complex tropical forests

The first forest gap model JABOWA (Botkin et al., 1972) was designed for a temperate forest. It provided a baseline for the now well-established forest gap modeling paradigm. Gap models share the following principles (Bugmann, 2001):

(i) Forests are represented as a collection of small patches. The forest successional stage and age vary across patches.
(ii) Patches are independent of their neighborhoods and do not interact with other patches. Thus, dynamic processes such as tree recruitment, growth and mortality are calculated separately for each patch.
(iii) All patches are homogeneous in size and resource level (i.e., light reaching the upper canopy). The size of one patch is usually chosen according to the extent of the largest possible tree crown (e.g., 20 m × 20 m). Intra- or interspecific interactions are simulated for all trees in a patch rather than tree-by-tree as tree positions are not included.
(iv) Leaves are modeled as thin disks on top of each tree. Trees standing within one patch compete for light due to asymmetric shading effects of larger tree canopies on smaller ones.

Many forest gap models were developed following the same principles (Bugmann, 2001; Bossel and Krieger, 1994; Yan and Shugart, 2005; Köhler and Huth, 1998). For example, in the FORET model, the concepts of JABOWA were adapted to simulate the diverse forests of the southern United States (Shugart and West 1977). The FORSKA (Prentice and Leemans, 1990) and FORCLIM models (Bugmann, 1996b) adopted the gap model approach to simulate forest dynamics of temperate forests in Europe. Building on the FORET model, the FORICO model was one of the first tropical forest gap models, which was applied in a lower montane rainforest in Puerto Rico (Doyle, 1981). Later, following the gap model approach FORMIX was applied to tropical forests in South-East Asia (Bossel and Krieger, 1991, 1994; Ditzer et al., 2000). FORMIX accounts for biomass and tree numbers in five distinct canopy layers (each layer has some representative trees similar to size class models).

FORMIND is the process- and individual-based successor of the FORMIX model, in which the concept of distinct layers was discarded. FORMIND was developed in the late 1990's to simulate tropical forest dynamics more realistically than before (Köhler and Huth, 1998, 2004; Köhler et al., 2000; full publication list see Appendix A). Within FORMIND, physiological processes such as photosynthesis and respiration are simulated at the tree level (process-based model). Forests of several hundred hectares can be simulated over a time period of a few centuries. The simulation area is a composite of 20-m × 20-m patches typical for forest gap models. In FORMIND, these patches may interact via seed dispersal and the falling of large trees. The basic model consists of four main processes: tree growth, tree mortality, recruitment of tree seedlings and competition between trees (Fig. 1, full model description see Appendixes B–F). Due to its main application in tropical forests lacking any pronounced seasonal cycle, the model architecture is based on a time step of one year. In the following, we discuss the main processes included in FORMIND.

Tree growth. Tree biomass growth is determined by a physiology-based tree carbon balance that includes leaf photosynthesis, maintenance and growth respiratory costs. An increase in tree biomass results in increments in height, stem diameter, stem volume and leaf area through the use of allometric relationships (see Appendix G for details).

Tree mortality. In FORMIND, background mortality is generally calculated stochastically from a mean annual mortality rate. Alternatively, the model also allows calculating mortality as a function of tree size or stem diameter growth. In addition, trees compete for space. Crowded stands are thinned, i.e., mortality rate is increased if crowns of trees overlap. If large trees die, they have a certain probability of falling over into neighboring patches, in which their crowns smash smaller trees and create canopy gaps. Thus, trees might die for various reasons (age, growth rate, space competition, tree fall damage; see also Appendix E for details). All individual tree mortalities are determined stochastically.

Recruitment. In FORMIND, trees emerge from seeds, which can originate either from a surrounding forest (constant seed rain) or from mother trees within the same forest stand. As seeds need a certain amount of light to germinate, their development might be hindered by shading effects on the forest ground. In that case, seeds are accumulated in the soil of a patch (seedbank) for a certain time until the light conditions are appropriate for germination. While waiting for better light conditions, a fraction of the seeds die (seed mortality). As soon as the light conditions change (e.g., through

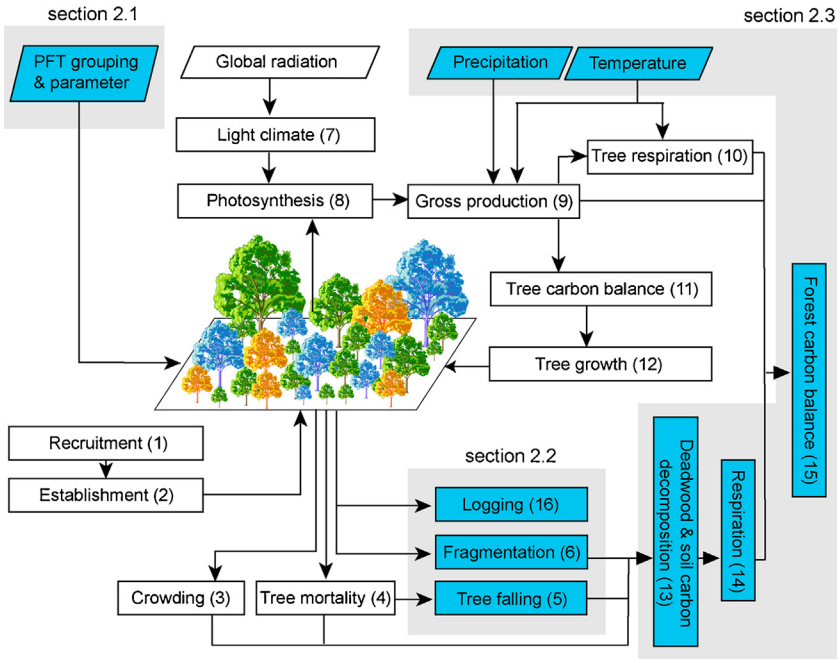

Fig. 1. The basic concept of FORMIND (white) and its extensions required for certain applications (blue). Boxes show physiological and demographic processes with numbers in brackets representing their scheduled flow. Parallelograms indicate important information needed as input for the model. Light gray boxes refer to sections in this manuscript that provide more details of the extensions. (For interpretation of the references to color in this figure legend, the reader is referred to the web version of this article.)

gap creation), seeds can receive sufficient light to germinate (see Appendix D for more details).

Tree competition. In FORMIND, the competition between individual trees is threefold. First, tree growth is mainly driven by light. Large trees in a patch receive most of the incoming radiation and gradually shade smaller trees, causing asymmetric light competition. Second, trees compete symmetrically for space. Trees in crowded patches are thinned by increasing mortality (Köhler et al., 2001). Third, between neighboring patches, the gap created by the falling of large trees increases the local mortality rates. Furthermore, seed dispersal from mother trees leads to interactions among patches (see Appendix F for more details).

Each modeled process is flexible enough to be parameterized for a specific study site. It takes a site specific forest inventory (including stem diameter measurements) and stem diameter increment measurements to obtain values for model parametrization. For site-specific adaptation of the model additional information is helpful. Uncertain parameter values can be determined by a calibration process using as reference inventory data of mature forests (e.g. in some studies this has been done for the recruitment rates). However, many parameters used in the model are known from literature (at least their typical ranges). For example, in tropical forests, approximately 1–2% of the standing trees die annually (Phillips and Gentry, 1994). In the case of site specific measurements, these parameters can be adapted.

Beside the modeled processes, three important aspects are incorporated into FORMIND which are intended to be applicable to tropical forest sites. This distinguishes FORMIND from classical forest gap models:

(1) The high tree species-richness in tropical forests is accounted for by the concept of plant functional types (PFTs), i.e., grouping of tree species (see Section 2.1).
(2) Disturbances, both on small and large scale, caused by either natural reasons (e.g. tree falling, edge effects) or anthropogenic activity (e.g. tree logging) are investigated on their effects on forest structure and dynamics (see Section 2.2).
(3) The simulation of the carbon balance of individual trees is based on a detailed process-based approach that enables upscaling to forest-wide carbon balances (see Section 2.3).

2.1. Consideration of tree species-rich forests: Plant functional types

Tropical forests have high tree species richness with up to 300 tree species per hectare (Whitmore, 1998; Slik et al., 2015). Modeling complex interactions between multiple tree species is important to reproduce typical emerging forest structures such as tree size distribution, species composition and aboveground forest biomass (Köhler and Huth, 1998). However, including this complexity (1) increases the effort for model parameterization, and (2) increases model uncertainty for the lack of empirical data for most tree species. To reduce model complexity, it is necessary to aggregate the hundreds of tree species into a few classes or types in a meaningful way. Field studies revealed that species often show similar attributes (e.g., growth rate, seed production rates, mortality rates), making it possible to classify similar tree species of highly diverse tropical forests into species groups known as plant functional types (PFT; Smith and Shugart, 1997). Following this knowledge, in one of the first FORMIND studies, all recorded tree species were aggregated into five or 22 PFTs to analyze the impact of species aggregation on tree competition and forest dynamics (Köhler and Huth, 1998). Although five PFTs were considered sufficient to reproduce more aggregated variables such as stem size distribution or basal area (Köhler et al., 2001), a higher number of PFTs is needed to represent interspecific competition and extinction processes. The initial concept of grouping tropical tree species into PFTs was later-on generalized in Köhler et al. (2000) based on the two physiological attributes maximum tree height at maturity and light requirement (or shade tolerance), that are assumed to be independent from each other. In the application of this grouping

concept for tropical lowland rainforest in South–East Asia, three different shade tolerance levels (shade-intolerant, intermediate and shade-tolerant species) and five different height groups of adult trees (shrubs, understory, lower and upper canopy, and emergent species) have been distinguished leading finally to 13 PFTs that can be found in tree species inventories (Köhler et al., 2000).

Note that finding a suitable number of PFTs for a specific research question of a simulation study is not completely resolved (Kazmierczak et al., 2014) and there are challenges to transfer the PFT classification to other regions (Bugmann, 1996a; Picard and Franc, 2003). Additionally, species classifications might not be unique for a certain study region as shown by Picard et al. (2012). In this study five different classification schemes were compared for the same tropical forest in French Guiana: the schemes agreed on the tree height classification but differed with respect to the light requirements of the trees.

Köhler and Huth (2007) showed that this PFT grouping might also be used to investigate questions on tropical tree species richness. They simulated the forest dynamics and species competition of a tropical rainforest in South–East Asia with more than 400 tree species using the PFT-based parameterization as published before (Köhler and Huth, 2004). However, tree regeneration including seed production was determined not for PFT, but tree species specific. The study explored how recruitment limitation (Hubbell et al., 1999) and disturbance intensity (i.e. intermediate disturbance hypothesis; Connell, 1978) influence tropical tree species richness. Köhler and Huth (2007) demonstrated that both processes are important for species richness in tropical forest. In addition, both processes interact, and should therefore not be analyzed separately. At a local level, an increase in recruitment limitation promotes species richness, whereas the overall richness at the forest level declines.

In general, to tackle the high tree species richness in tropical forests, species grouping offers a powerful technique to reduce complexity. In applications with FORMIND, we have shown that this approach allows a realistic description of species dynamics in forests (e.g., Köhler and Huth, 1998). The creation of these functional groups is flexible enough to include relevant differences and to avoid functional redundancy between species (Kazmierczak et al., 2014). Future research could tackle the question of how many PFTs are appropriate to describe a specific forest (e.g., Picard et al., 2012). The results of future research in the field of functional biodiversity can be used to improve the species grouping concept of forest models.

2.2. The impact of disturbances and logging on forest dynamics

Disturbance regimes and forest management play an important role for forests dynamics. Disturbances can occur on varied spatial scales. Large-scale disturbances occur across several hectares (e.g., wildfire) and small-scale (local) disturbances occur within a few meters (e.g., falling trees). Most gap models incorporate natural disturbances, e.g., the falling of large trees, which creates new forest gaps. This tree fall process was included in FORMIND, including physical damages caused to surrounding trees. Surrounding trees (in the same or neighboring patches) are damaged depending on the crown size of the falling tree and their own height (for details see Appendix E.3).

In addition to natural disturbances, logging poses a major threat to tropical forests. One challenge is to evaluate whether a certain forest management practice is sustainable. Logging has been included in FORMIND, allowing users to simulate different logging strategies and to explore their long-term impacts on forest dynamics (Kammesheidt et al., 2001; Köhler and Huth, 2004). The individual-based approach easily allows selecting single trees and removing them from the forest. Such a selection of single trees for logging typically depends on species group and stem diameter (cutting limits). FORMIND provides two logging strategies: conventional logging and reduced impact logging (RIL). RIL takes into account substantial planning of the logging event. This refers mainly to the direction in which the logged tree falls, i.e., toward the largest gap, which reduces the damage and thus death of other trees. Consequently, the falling tree causes the least amount of damage to surrounding trees. The damage caused to surrounding trees is similar to the natural tree falling (see above), but includes an additional damage due to road building efforts etc. (for details see Appendix I).

Using FORMIND, simulation studies conducted in Venezuela (Kammesheidt et al., 2001) and Malaysia (Köhler and Huth, 2004; Huth et al., 2004, 2005) showed the impact of different management strategies on the yield and forest state. It was shown that long logging cycles (>60 years) in combination with reduced-impact logging strategies could significantly reduce the negative long-term impact of logging on forest carbon stocks. This strategy might be applied as a compromise between economic and ecological interests (Huth et al., 2005). The results from another study conducted in rainforests in South America demonstrated that legal logging strategies (i.e., strip cuttings) severely altered the structure and composition of old-growth stands (Rüger et al., 2007). Alternative logging strategies that compromise between ecological and economic interests have been proposed, for example, reliance on native species and retention of an uneven-aged forest structure. This proposed strategy promotes the maintenance of native biodiversity and tree reproduction, and protects the forest ecosystem from exotic species invasion (Rüger et al., 2007). Similar studies have been conducted to investigate logging for forest sites in Mexico (Rüger et al., 2008), Malaysia (Ditzer et al., 2000; Glauner et al., 2003; Tietjen and Huth, 2006; Huth and Ditzer, 2001), Venezuela (Kammesheidt et al., 2001) and Paraguay (Kammesheidt et al., 2002). Based on these simulation experiments, an attempt was made to estimate thresholds for logging intensities to maintain a stable forest structure and species composition.

While logging can affect forest structure, forest conversion into agricultural land leads to forest fragmentation (Skole and Tucker, 1993; Laurance et al., 1998). Empirical studies showed that forest fragments suffer from edge effects up to 300 m into the forest (Laurance et al., 2002). These edge effects induce changes in the microclimate, resulting in higher tree mortality (Laurance et al., 2002). Therefore, such edge effects, i.e., higher mortality rates in the edge area of a fragment, have been introduced into FORMIND by increasing the background mortality and introducing extra mortality for large trees within the first 100 m of the forest edge to represent changes in micro-climatic conditions and the impact of wind turbulence (see Appendix E.4 for more details). Simulations of forest fragmentation using FORMIND for forest stands in French Guiana and the Mata Atlantica showed that standing forest biomass was significantly reduced by up to 60% compared with non-fragmented forests (Pütz et al., 2011; Köhler et al., 2003).

Simulating small isolated forest fragments instead of continuous forests requires a concept of local tree regeneration. In this context we differentiate between two seed dispersal modes: (1) local dispersal, i.e. all seedlings are originated from fertile trees within the simulated area and (2) external seed rain. Furthermore, Groeneveld et al. (2009) found that negative density regulation for seedlings was necessary to match empirical data from the Brazilian Atlantic rainforest. We have found that moderate density regulation is essential to achieve coexistence for a broad range of regeneration parameters. This ecological process is essential to increase structural realism when analyzing the impacts of forest fragmentation. Without density regulation coexistence would be only possible in the model for a small range of the regeneration parameters, which

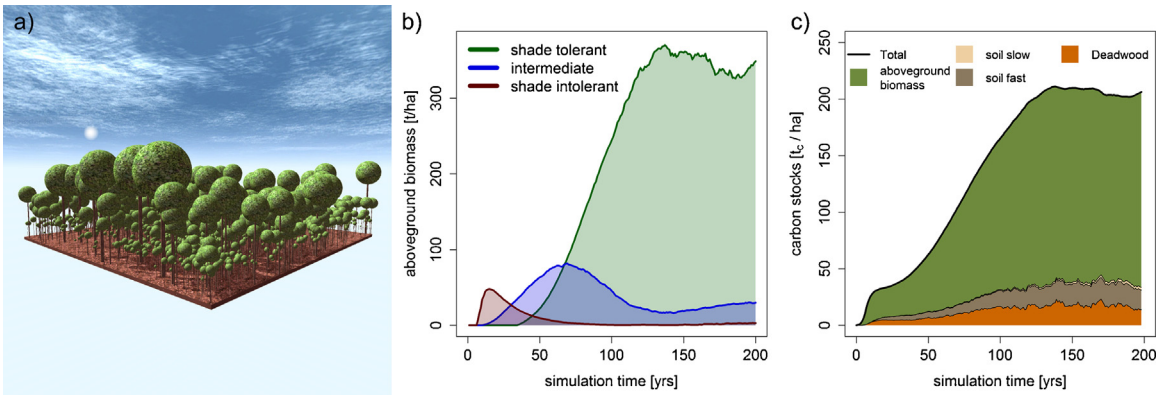

Fig. 2. Forest succession and carbon stocks simulated using FORMIND. (a) Exemplary visualization of a simulated forest stand showing all trees with a stem diameter >10 cm for a forest area of 1 ha. (b) Simulated forest succession of a tropical forest with a size of 1 ha on Mt. Kilimanjaro, Tanzania. We distinguished between shade-tolerant tree species (climax species), shade-intolerant tree species (pioneer species) and intermediate shade-tolerant species (Fischer et al., 2015). (c) Simulated amount of carbon in the living biomass, in the deadwood, and in the soil (fast and slow decomposing soil stock) for a tropical forest on Mt. Kilimanjaro, Tanzania (Fischer et al., 2015).

seems to be unrealistic and does not reflect the large variability in field measurements.

A study of the long-term degradation trajectory of initially undisturbed forest fragments within the Atlantic Forest showed that increased tree mortality is the most important fragmentation process acting on forest edges (e.g., due to changes in seed dispersal and micro climate; Pütz et al., 2011). Simulations with FORMIND showed that the degradation process occurring in fragmented forests might last for approximately a century, and might result in aboveground carbon losses of more than 5 Mg C ha^{-1} y^{-1}, and changes in evapotranspiration (43% loss) and surface runoff (57% gain) at forest edges (Dantas de Paula et al., 2015).

In a nutshell, as the impact of disturbance events in forests is mainly quantified at the tree level, an individual-based structure is a huge advantage for simulating disturbances. This structural realism was the key driver for the successful application of the gap model FORMIND for questions on forest management and fragmentation. Other types of disturbances, such as landslides, forest wildfires, and windstorms, have also been found important to increase structural realism of FORMIND (e.g., Rüger et al., 2007; Gutiérrez and Huth, 2012; Dislich and Huth, 2012). An unanswered question remains on how to upscale the forest gap models to larger areas. For fragmentation one approach to link forest gap models to remote sensing data for the whole Amazon rainforest has been developed (see below). There is a strong need to develop methods for a further integration of remote sensing and the simulation of forest dynamics (Shugart et al., 2015).

2.3. Simulating the carbon balance of tropical forests

The carbon balance of a tropical forest depends on its successional stage and the environmental conditions. Hence, the carbon budget is variable at the local scale and forests might be a source or a sink of atmospheric CO_2 (Gatti et al., 2014; Morton et al., 2014). To simulate the carbon balance of an entire forest, a physiological approach based on the growth of every single tree is essential. Including this approach into FORMIND, it offers the possibility for simulating the forest carbon balance at different successional stages and under variable climate conditions as the model calculates the carbon balance for each individual tree.

2.3.1. Carbon balance in a forest gap model

In contrast to many other forest gap models, FORMIND calculates the biomass increment via a tree carbon balance based explicitly on photosynthetic production and respiratory losses (Thornley and Johnson, 1990). Biomass production leads to tree growth, which is predominantly driven by light in FORMIND (details in Appendix G). Photosynthesis is calculated based on light availability within the forest canopy (Thornley and Johnson, 1990), whereby large trees shade smaller ones that grow in the same forest patch. This assumption differs from biogeochemical models in which the assimilation of atmospheric CO_2 is based on carbon pools at the ecosystem level (e.g., dynamic global vegetation model LPJ, Sitch et al., 2003). In FORMIND, respiratory costs are assumed to be tree-size dependent. Recently, the model was extended to incorporate the decomposition processes of deadwood and soil carbon (see Fig. 2; Details see Appendix H; Gutiérrez, 2010; Fischer et al., 2014, 2015). The sum of these above- and belowground fluxes contributes to a more complete assessment of the carbon balance in forest ecosystems (Figs. 2 and 3) and helps to identify the role of successional stages in the local and regional carbon cycle and how it might contribute to the global carbon budget. This approach allows simulation experiments and complements complex field measurements (e.g., based on eddy-covariance techniques).

2.3.2. The impact of climate change on tropical forests

The influence of climate changes on forest carbon stocks and fluxes remains highly uncertain (Wang et al., 2014). The physiological approach, as used in FORMIND, enables investigation of the influence of variable climate conditions on the carbon balance of forest ecosystems. Several modules were implemented in FORMIND by adopting the growth of single trees with respect to climatic changes: temperature limitations of photosynthesis and respiration (approaches from: Haxeltine and Prentice, 1996; Prentice et al., 1993) and the influence of the soil water content on photosynthesis (Details see Appendix F.2; Fischer et al., 2014; Gutiérrez et al., 2014). The effect of changes in precipitation on tropical forests was analyzed in a case study conducted in Madagascar (Fischer et al., 2014). A decline in rainfall by more than 30% reduced biomass by 20% and drought-intolerant species almost went extinct. These effects can be amplified by additional stress factors, such as rising temperatures or tree harvesting. For rainforests in South America, FORMIND simulations suggested that primary old-growth forests will be reduced in aboveground biomass by 11% whereas the net primary productivity might decrease by 30% in the year 2100 due to increased drought conditions (Gutiérrez et al., 2014).

2.3.3. The carbon balance of tropical forests at a biome scale

Given the increasing availability of remote sensing data (e.g. Ribeiro et al., 2009), FORMIND was recently applied at a regional scale (i.e., the Amazon forest) by combining local ecological

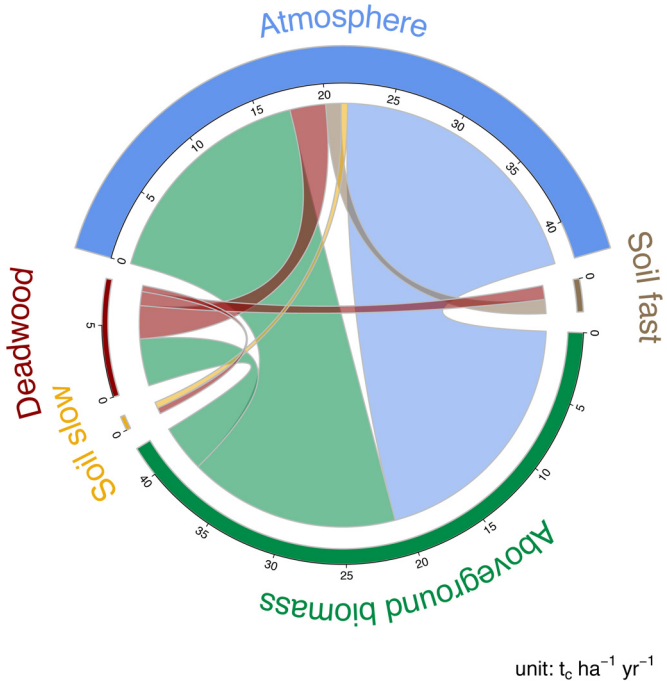

Fig. 3. Example of simulated forest carbon fluxes. The mean carbon fluxes of a simulated old-growth tropical forest on Mt. Kilimanjaro, Tanzania, are presented (Fischer et al., 2015). The colors indicate the different stocks and fluxes. The color of the fluxes indicates the source of the flux. From the atmosphere (blue), the greatest flux goes to aboveground biomass (forest gross primary productivity). Aboveground biomass (green) emits carbon back to the atmosphere due to tree respiration, and biomass mortality to the deadwood pool. From the deadwood pool (red), carbon is emitted to the atmosphere or to a slow (yellow) or fast (brown) decomposing soil carbon stock. Carbon is emitted to the atmosphere from both soil stocks. The amount of carbon in the different fluxes is indicated by the thickness of the colored links; the amount of carbon stored in the different stocks is indicated by the thickness of the circle frame pointing inwards. The circle frame of the atmosphere points outwards because carbon moves from the atmosphere to the forest. (For interpretation of the references to color in this figure legend, the reader is referred to the web version of this article.)

knowledge with remote sensing data on forest patch structures (Pütz et al., 2014). This analysis of the long-term dynamics of forest fragments in South America (i.e., long-term carbon loss per fragment for different fragment sizes) revealed that small fragments lose approximately 50–60% of the aboveground carbon stored in living trees. This study provides a first estimate of land carbon losses of about 0.25 Pg C per year due to forest fragmentation in the tropics (see Fig. 4; Pütz et al., 2014). Losses caused by fragmentation contribute approximately 25% to the total carbon loss due to land use change and are therefore important for a comprehensive understanding of the role of vegetation dynamics within the global carbon cycle (Pütz et al., 2014).

The example of FORMIND shows how additional process-based elements can be implemented into forest gap models. To conclude, the structural realistic description of tree-related processes has various advantages: (1) processes and parameters have a physical or physiological interpretation, (2) model parameters can be measured in field experiments, and (3) model structure is flexible enough to adapt processes to new circumstances (e.g., climate change) or to include new processes (e.g., logging). The process-based and individual-based approach of FORMIND allows the calculation of gross primary production and respiration of forests, which is not possible with classical gap models. This offers the possibility of quantifying the carbon fluxes of forests at different scales and linking these fluxes to dynamics in the forest. This is a result of the individual-based structure of forest gap models, which is the basis for linking forest carbon balance to tree competition. In addition, the individual-based approach allows integrating various types of disturbance regimes.

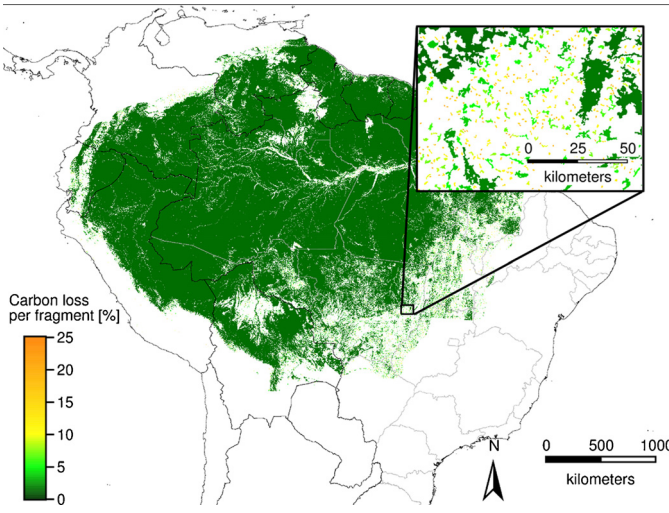

Fig. 4. Spatial distribution of tropical forest fragments in the Amazon Forest and their estimated carbon loss due to fragmentation. Color ranges indicate the relative carbon loss due to fragmentation, which was estimated using the FORMIND model (Pütz et al., 2014).

3. Current and future applications of forest gap models

Having summarized how a forest gap model has been developed for the tropics over the last decades, we now provide a brief outlook on new applications.

Forest gap models can be used to study the relationship between forest productivity and tree species diversity (Morin et al. 2011). Recent studies have shown that forest productivity typically increases with increasing tree species diversity (e.g., Morin et al. 2011; Zhang et al., 2012; Vilà et al., 2007). However, several studies show unchanged or even inverse relationships between productivity and diversity (e.g., Jacob et al., 2010; Cavard et al., 2010). Following the study of Morin et al. (2011), we extended this method to study a broader range of diversity-productivity relationships. Instead of long-term simulations, thousands of different virtual forest stands have been generated, combining different species mixtures with various forest structures (e.g., different basal area values or heterogenic tree heights). For each of these virtual forest stands, forest productivity can be calculated using forest gap models. The obtained diversity - productivity relationships can then be compared to field studies. This new way of using a forest gap model as an analysis tool of virtual forest stands enables a much faster analysis of numerous forests compared with the classical method of simulating forest successions.

Parameter estimation in forest gap models is a challenging process. Manual calibration and sensitivity analysis of these models require a large number of simulations, leading to a time-consuming computational demand. Thus, for the automatic calibration of uncertain parameters, when direct measurements are missing or made under specific conditions (e.g., climate, soil), a collection of rapid stochastic search methods have been developed (Tolson and Shoemaker, 2007) and applied in FORMIND (Lehmann and Huth, 2015). These methods automatically minimize the difference between simulation results and field observations by running the model a thousand times. Additionally, for the assessment of parameter uncertainty, approximate Bayesian methods can be used in combination with a Markov chain Monte Carlo approach (Hartig et al., 2011). These methods can also be used for forest sites where a limited number of observations in time and space are available

After careful examination of the model and available observation data, a combination of manual and automatic calibrations leads to the successful parameterization of forest gap models.

A very recent and promising application of forest models is in combination with remote sensing data. Techniques such as Radar (Radio detection and ranging) and Lidar (Light detection and ranging) are capable of measuring the 3D-structures of forests. However, the intrinsic attributes of the forests, such as biomass, can only be estimated indirectly with remote sensing based on empirical relationships (e.g., Drake et al., 2002; Asner, 2009; Lefsky et al., 2002). The calibration of such relationships has long been limited by the availability of field data and the spatial resolution of remote sensing data, especially in the tropics. Synthetic forest inventory data generated by forest models provide a novel approach to explore forest structures and develop new concepts for remote sensing (Palace et al., 2015). To this end, the full functionality of an individual-based forest model might be used, including the simulation of disturbances, topographic variability and carbon fluxes (Shugart et al., 2015). The classical method is to use remote sensing data to set the initial state of forest models. Here, forest gap models are used the other way around to calibrate remote sensing products by creating virtual remote sensing flights over simulated forests. So far, FORMIND has served to investigate the relationship between canopy height and aboveground biomass as a function of spatial scale (Köhler and Huth, 2010). In the near future, FORMIND will also be used to improve the understanding of the relationship between forest structure and other ecosystem functions, e.g., forest productivity. Until now, remote sensing efforts toward the detection of changes in biomass content in the tropics have been restricted to a few sites (Dubayah et al., 2010; Englhart et al., 2013; Meyer et al., 2013). By using forest models, general principles might be found, on which one might base new remote sensing applications.

4. Discussion

Finding an acceptable balance between model simplicity and required complexity is a classic challenge in ecological modelling (Grimm et al., 2005; Evans et al., 2013). In this review, we showed how the FORMIND model could achieve this balance by combining the gap approach with fundamental ecological processes. The individual-based structure of forest gap models allows the modeling of structural realistic concepts that are based on field measurements at different organizational levels (e.g., leaves, trees, forests). Forest ecosystem functions (e.g., productivity) and forest structure (e.g., tree size distribution) emerge from individual trees and their interactions. Using the forest gap model FORMIND as an example, it was demonstrated that whenever a new ecological pattern was investigated, the basic concept of the model did not change; rather, a new module was added. The use of the same model, but with the addition of modules instead of the construction of new models for different applications, allowed a rigid comparison of results and fostered theory development. In particular, we highlighted the advances that have been made in the fields of (1) species aggregation using PFTs, (2) modeling the impact of natural and anthropogenic disturbances on ecosystem functions and forest dynamics, and (3) upscaling carbon dynamics from photosynthesis at the leaf level to the forest ecosystem level.

Such extensions have led to a modular architecture of forest gap models, which allowed FORMIND to be successfully applied to different forest sites worldwide during the last two decades (Fig. 5). This modular architecture began with the development of logging routines to simulate the impact of tree harvesting on forest structure. Later applications provided insights into the role of forest fragmentation within the global carbon cycle. In particular, the individual-based structure of gap models facilitates modelling the impact of disturbances, such as logging, on forest dynamics. Studies on the effects of human activities and recently, changing climatic conditions, have motivated extensions of FORMIND toward a complete forest carbon balance model.

In summary, during the last two decades, FORMIND has shown that forest gap models can be applied to tropical forest sites and that such models are capable tools to provide answers to questions related to species richness, natural and anthropogenic disturbances, and carbon balance (Fig. 6; a full list of all FORMIND related publications can be found in Appendix A). We envision a strong potential of forest gap models in the future, i.e., with respect to the coupling of these models to remote sensing data due to the increasing availability of various products and new missions.

Forest gap models such as FORMIND, ForClim (Bugmann and Solomon, 2000), FAREAST (Yan and Shugart, 2005), and ZELIG (Urban et al., 1991) are usually applied at the local scale (e.g., hundreds of hectares), although most of them can simulate forest dynamics for a wide range of different environmental conditions. In contrast, dynamic global vegetation models (DGVMs) have been designed to simulate forest dynamics at a regional to global scale (e.g. LPJ-DGVM or SEIB–DGVM: Sitch et al., 2003; Sato et al., 2007), but are limited by necessary simplification of ecological processes. Note that forest gap models and DGVMs have been developed to address different research questions. While forest gap models focus

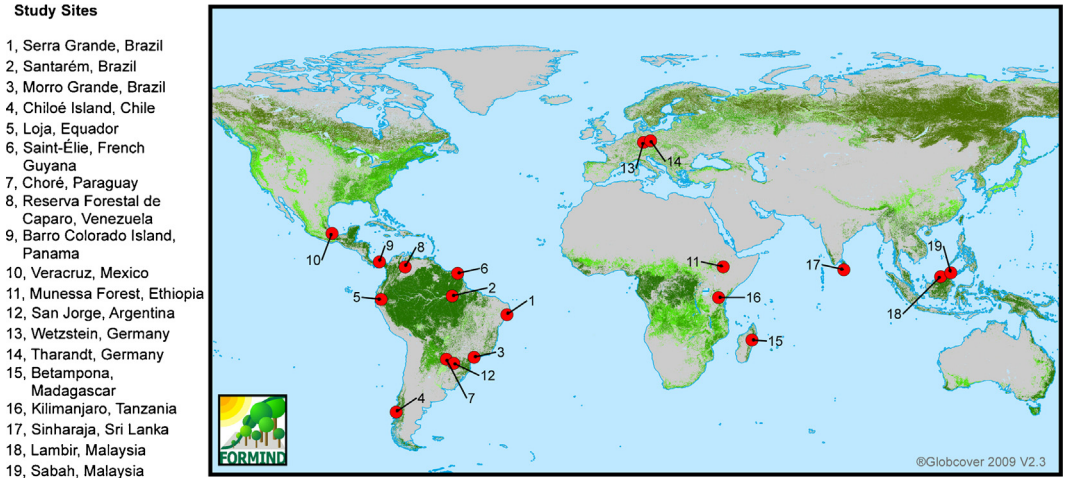

Fig. 5. Study sites to which the FORMIND model family has been applied (including also applications beyond the tropics).

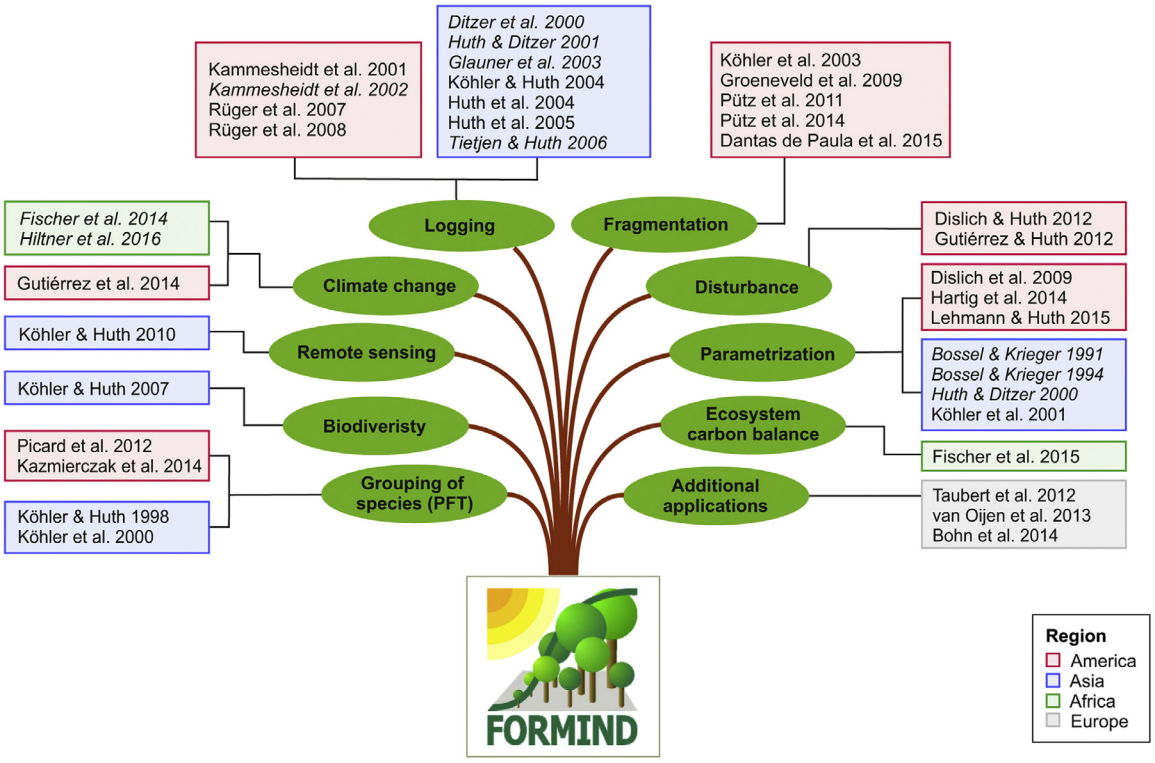

Fig. 6. Overview of studies using models of the FORMIND model family. Publications are ordered by research field and study region. A full list with all publications can be found in the Appendix A including the specific research topic, study region and forest type. 'Additional applications' include FORMIND model versions developed for temperate forests and grasslands. Publications of the related FORMIX model are shown in italics.

on reproducing forest structure and dynamics at the local scale, DGVMs have been used to project global change in vegetation cover and aboveground carbon stocks at coarse resolution (Sitch et al., 2003). At the global scale, DGVMs have to reduce species diversity to a few broadly classified plant functional types (PFTs). For example, in most DGVMs, only one dominating PFT is used to describe tropical forests at the cost of a realistic reproduction of forest succession. Attempts to include the individual-based approach into DGVMs have already been made, for example, in the SEIB-DGVM model (Sato et al., 2007) and the LPJ-GUESS model (Hickler et al., 2012; Wårlind et al., 2014). However, large-scale applications could still benefit from embedding more concepts of forest gap models into the DGVM framework. Landscape forest models such as LandClim (Schumacher et al., 2004; Schumacher, 2004) try to transfer the gap model concept to landscapes (e.g., for 10,000 ha) including explicit position of gaps and seed dispersal (similar to FORMIND). This type of approach has potential to be applied also on larger scales at the cost of increasing simulation times. To describe the impact of disturbances (e.g., fire, logging) or land-use change on forests across spatial scales the individual-based approach of gap models is a strong advantage. For future model developments and large-scale applications, we suggest developing methods for upscaling local gap models or embedding forest gap models in DGVMs (see also Snell et al., 2014).

The individual-based approach of forest gap models offer a high degree of flexibility to be adapted to different environments (e.g., temperate, sub-tropical, cloud forests) or even other ecosystem types (e.g., temperate grassland; Taubert et al., 2012; Coffin and Lauenroth, 1990). This high flexibility has motivated the increasing number of simulation studies using forest gap models like the FORMIND model (Fig. 5). During the development of forest gap models, extensive knowledge has been gathered on modelling processes in forests, their parameterization and resulting model behavior. For the evolution of such complex simulation models, this learning process has been highly relevant. As a side effect, future model applications have already been initiated (e.g., link to remote sensing), which in turn might feed back into the design of new field experiments and monitoring studies, or hypothesis building in forest ecology. Therefore, both field experiments as well as theoretical forest ecology might benefit from the application of forest gap models. This closer connection promotes a better understanding of the role of complex forest ecosystems on Earth, which in future will become more relevant to a society under global change.

Acknowledgements

We want to thank Felix May and Ulrike Hiltner for helpful discussions on the manuscript. The authors also want to thank the anonymous reviewers for their valuable comments. RF, FB, SeP and AH were supported by the Helmholtz-Alliance Remote Sensing and Earth System Dynamics. AH and SaP were supported by the ERC advanced grant 233066. AGG was funded by a DAAD doctoral fellowship. NK was funded by the German Federal Ministry for Economic Affairs and Energy (BMWi) under the funding reference 50EE1416.

Appendix A-J. Supplementary data

Supplementary data associated with this article can be found, in the online version, at http://dx.doi.org/10.1016/j.ecolmodel.2015.11.018.

References

Anderson-Teixeira, K.J., Davies, S.J., Bennett, A.C., Gonzalez-Akre, E.B., Muller-Landau, H.C., Wright, J.S., Abu Salim, K., Almeyda Zambrano, A.M., Alonso, A.

Baltzer, J.L., Basset, Y., Bourg, N.A., Broadbent, E.N., Brockelman, W.Y., Bunyavejchewin, S., Burslem, D.F.R.P., Butt, N., Cao, M., Cardenas, D., Chuyong, G.B., Clay, K., Cordell, S., Dattaraja, H.S., Deng, X., Detto, M., Du, X., Duque, A., Erikson, D.L., Ewango, C.E.N., Fischer, G.A., Fletcher, C., Foster, R.B., Giardina, C.P., Gilbert, G.S., Gunatilleke, N., Gunatilleke, S., Hao, Z., Hargrove, W.W., Hart, T.B., Hau, B.C.H., He, F., Hoffman, F.M., Howe, R.W., Hubbell, S.P., Inman-Narahari, F.M., Jansen, P.A., Jiang, M., Johnson, D.J., Kanzaki, M., Kassim, A.R., Kenfack, D., Kibet, S., Kinnaird, M.F., Korte, L., Kral, K., Kumar, J., Larson, A.J., Li, Y., Li, X., Liu, S., Lum, S.K.Y., Lutz, J.A., Ma, K., Maddalena, D.M., Makana, J.R., Malhi, Y., Marthews, T., Mat Serudin, R., McMahon, S.M., McShea, W.J., Memiaghe, H.R., Mi, X., Mizuno, T., Morecroft, M., Myers, J.A., Novotny, V., De Oliveira, A.A., Ong, P.S., Orwig, D.A., Ostertag, R., den Ouden, J., Parker, G.G., Phillips, R.P., Sack, L., Sainge, M.N., Sang, W., Sri-Ngernyuang, K., Sukumar, R., Sun, I.F., Sungpalee, W., Suresh, H.S., Tan, S., Thomas, S.C., Thomas, D.W., Thompson, J., Turner, B.L., Uriarte, M., Valencia, R., Vallejo, M.I., Vicentini, A., Vrška, T., Wang, X., Wang, X., Weiblen, G., Wolf, A., Xu, H., Yap, S., Zimmerman, J., 2015. CTFS-ForestGEO: a worldwide network monitoring forests in an era of global change. Global Change Biol. 21, 528–549.

Asner, G.P., 2009. Tropical forest carbon assessment: integrating satellite and airborne mapping approaches. Environ. Res. Lett. 4, 4.

Bonan, G.B., 2008. Forests and climate change: forcings, feedbacks, and the climate benefits of forests. Science 320, 1444–1449.

Bossel, H., Krieger, H., 1991. Simulation model of natural tropical forest dynamics. Ecol. Modell. 59, 37–71.

Bossel, H., Krieger, H., 1994. Simulation of multi-species tropical forest dynamics using a vertically and horizontally structured model. For. Ecol. Manage. 69, 123–144.

Botkin, D.B., Janak, J.F., Wallis, J.R., 1972. Some ecological consequences of a computer model of forest growth. J. Ecol. 60, 849–873.

Bugmann, H., 1996a. Functional types of trees in temperate and boreal forests: classification and testing. J. Veg. Sci. 7, 359–370.

Bugmann, H., 1996b. A simplified forest model to study species composition along climate gradients. Ecology 77, 2055–2074.

Bugmann, H., 2001. A review of forest gap models. Clim. Change 51, 259–305.

Bugmann, H., Solomon, A.M., 2000. Explaining forest composition and biomass across multiple biogeographical regions. Ecol. Appl. 10, 95–114.

Cavard, X., Bergeron, Y., Chen, H.Y.H., Paré, D., 2010. Mixed-species effect on tree aboveground carbon pools in the east-central boreal forests. Can. J. For. Res. 40, 37–47.

Ceballos, G., Ehrlich, P.R., Barnosky, A.D., García, A., Pringle, R.M., Palmer, T.M., 2015. Accelerated modern human-induced species losses: entering the sixth mass extinction. Sci. Adv. 1, e1400253.

Coffin, D.P., Lauenroth, W.K., 1990. A gap dynamics simulation model of succession in a semiarid grassland. Ecol. Modell. 49, 229–266.

Connell, J.H., 1978. Diversity in tropical rain forests and coral reefs. Science 199, 1302–1310.

Dantas de Paula, M., Groeneveld, J., Huth, A., 2015. Tropical forest degradation and recovery in fragmented landscapes—Simulating changes in tree community, forest hydrology and carbon balance. Global Ecol. Conserv. 3, 664–677.

Debinski, D.M., Holt, R.D., 2000. A survey and overview of habitat fragmentation experiments. Conserv. Biol. 14, 342–355.

Dislich, C., Huth, A., 2012. Modelling the impact of shallow landslides on forest structure in tropical montane forests. Ecol. Modell. 239, 40–53.

Ditzer, T., Glauner, R., Forster, M., Köhler, P., Huth, A., 2000. The process-based stand growth model Formix 3-Q applied in a GIS environment for growth and yield analysis in a tropical rain forest. Tree Physiol. 20, 367–381.

Doyle, T.W., 1981. The role of disturbance in the gap dynamics of montane rain forest: an application of a tropical forest succession model. In: West, D.C., Shugart, H.H., Botkin, D.B. (Eds.), Forest Succession: Concepts and Application. Springer, New York, Heidelberg, Berlin, pp. 56–73.

Drake, J.B., Dubayah, R.O., Clark, D.B., Knox, R.G., Blair, J.B., Hofton, M.A., Chazdon, R.L., Weishampel, J.F., Prince, S.D., 2002. Estimation of tropical forest structural characteristics using large-footprint lidar. Remote Sens. Environ. 79, 305–319.

Dubayah, R.O., Sheldon, S.L., Clark, D.B., Hofton, M.A., Blair, J.B., Hurtt, G.C., Chazdon, R.L., 2010. Estimation of tropical forest height and biomass dynamics using lidar remote sensing at La Selva, Costa Rica. J. Geophys. Res. Biogeosci. 115, G00E09.

Englhart, S., Jubanski, J., Siegert, F., 2013. Quantifying dynamics in tropical peat swamp forest biomass with multi- temporal LiDAR datasets. Remote Sens. 5, 2368–2388.

Evans, M.R., Grimm, V., Johst, K., Knuuttila, T., de Langhe, R., Lessells, C.M., Merz, M., O'Malley, M.A., Orzack, S.H., Weisberg, M., Wilkinson, D.J., Wolkenhauer, O., Benton, T.G., 2013. Do simple models lead to generality in ecology? Trends Ecol. Evol. 28, 578–583.

Fischer, R., Armstrong, A., Shugart, H.H., Huth, A., 2014. Simulating the impacts of reduced rainfall on carbon stocks and net ecosystem exchange in a tropical forest. Environ. Modell. Softw. 52, 200–206.

Fischer, R., Ensslin, A., Rutten, G., Fischer, M., Schellenberger Costa, D., et al., 2015. Simulating carbon stocks and fluxes of an african tropical montane forest with an individual-based forest model. PLoS ONE 10 (4), e0123300, http://dx.doi.org/10.1371/journal.pone.0123300.

Gatti, L.V., Gloor, M., Miller, J.B., Doughty, C.E., Malhi, Y., Domingues, L.G., Basso, L.S., Martinewski, A., Correia, C.S.C., Borges, V.F., Freitas, S., Braz, R., Anderson, L.O., Rocha, H., Grace, J., Phillips, O.L., Lloyd, J., 2014. Drought sensitivity of Amazonian carbon balance revealed by atmospheric measurements. Nature 506, 76–80.

Gibson, L., Lee, T.M., Koh, L.P., Brook, B.W., Gardner, T.A., Barlow, J., Peres, C.A., Bradshaw, C.J.A., Laurance, W.F., Lovejoy, T.E., Sodhi, N.S., 2011. Primary forests are irreplaceable for sustaining tropical biodiversity. Nature 478, 378–+.

Glauner, R., Ditzer, T., Huth, A., 2003. Growth and yield of tropical moist forest for forest planning: an inquiry through modeling. Can. J. For. Res. 33, 521–535.

Grace, J., Mitchard, E., Gloor, E., 2014. Perturbations in the carbon budget of the tropics. Global Change Biol. 20, 3238–3255.

Grimm, V., Revilla, E., Berger, U., Jeltsch, F., Mooij, W.M., Railsback, S.F., Thulke, H.-H., Weiner, J., Wiegand, T., DeAngelis, D.L., 2005. Pattern-oriented modeling of agent-based complex systems: lessons from ecology. Science 310, 987–991.

Groeneveld, J., Alves, L.F., Bernacci, L.C., Catharino, E.L.M., Knogge, C., Metzger, J.P., Pütz, S., Huth, A., 2009. The impact of fragmentation and density regulation on forest succession in the Atlantic rain forest. Ecol. Modell. 220, 2450–2459.

Gutiérrez, A.G., 2010. Long-Term Dynamics and the Response of Temperate Rainforests of Chiloé Island (Chile) to Climate Change. Technische Universität München, Lehrstuhl für Waldwachstumskunde, pp. 170.

Gutiérrez, A.G., Armesto, J.J., Díaz, M.F., Huth, A., 2014. Increased drought impacts on temperate rainforests from southern South America: results of a process-based, dynamic forest model. PLoS ONE 9, e103226.

Gutiérrez, A.G., Huth, A., 2012. Successional stages of primary temperate rainforests of Chiloé Island. Chile Perspect. Plant Ecol. Evol. Syst. 14, 243–256.

Hansen, M.C., Potapov, P.V., Moore, R., Hancher, M., Turubanova, S.A., Tyukavina, A., Thau, D., Stehman, S.V., Goetz, S.J., Loveland, T.R., Kommareddy, A., Egorov, A., Chini, L., Justice, C.O., Townshend, J.R.G., 2013. High-resolution global maps of 21st-century forest cover change. Science 342, 850–853.

Hartig, F., Calabrese, J.M., Reineking, B., Wiegand, T., Huth, A., 2011. Statistical inference for stochastic simulation models—theory and application. Ecol. Lett. 14, 816–827.

Haxeltine, A., Prentice, I.C., 1996. A general model for the light-use efficiency of primary production. Funct. Ecol. 10, 551–561.

Hickler, T., Vohland, K., Feehan, J., Miller, P.A., Smith, B., Costa, L., Giesecke, T., Fronzek, S., Carter, T.R., Cramer, W., Kuhn, I., Sykes, M.T., 2012. Projecting the future distribution of European potential natural vegetation zones with a generalized, tree species-based dynamic vegetation model. Global Ecol. Biogeogr. 21, 50–63.

Hubbell, S.P., Foster, R.B., O'Brien, S.T., Harms, K.E., Condit, R., Wechsler, B., Wright, S.J., de Lao, S.L., 1999. Light-gap disturbances, recruitment limitation, and tree diversity in a neotropical forest. Science 283, 554–557.

Huston, M., DeAngelis, D., Post, W., 1988. New computer models unify ecological theory—Computer simulations show that many ecological patterns can be explained by interactions among individual organisms. BioScience 38, 682–691.

Huth, A., Ditzer, T., 2001. Long-term impacts of logging in a tropical rain forest—a simulation study. For. Ecol. Manage. 142, 33–51.

Huth, A., Drechsler, M., Köhler, P., 2004. Multicriteria evaluation of simulated logging scenarios in a tropical rain forest. J. Environ. Manage. 71, 321–333.

Huth, A., Drechsler, M., Köhler, P., 2005. Using multicriteria decision analysis and a forest growth model to assess impacts of tree harvesting in Dipterocarp lowland rain forests. For. Ecol. Manage. 207, 215–232.

IPCC, 2013. Climate change 2013: the physical science basis. In: Stocker, T.F., et al. (Eds.), Contribution of Working Group I to the Fifth Assessment Report of the Intergovernmental Panel on Climate Change. Cambridge University Press, Cambridge, United Kingdom and New York, NY, USA, p. 1535.

Jacob, M., Leuschner, C., Thomas, F.M., 2010. Productivity of temperate broad-leaved forest stands differing in tree species diversity. Ann. For. Sci. 67, 503.

Kammesheidt, L., Köhler, P., Huth, A., 2001. Sustainable timber harvesting in Venezuela: a modelling approach. J. Appl. Ecol. 38, 756–770.

Kammesheidt, L., Köhler, P., Huth, A., 2002. Simulating logging scenarios in secondary forest embedded in a fragmented neotropical landscape. For. Ecol. Manage. 170, 89–105.

Kazmierczak, M., Wiegand, T., Huth, A., 2014. A neutral vs. non-neutral parametrizations of a physiological forest gap model. Ecol. Modell. 288, 94–102.

Köhler, P., Chave, J., Riéra, B., Huth, A., 2003. Simulating the long-term response of tropical wet forests to fragmentation. Ecosystems 6, 114–128.

Köhler, P., Ditzer, T., Huth, A., 2000. Concepts for the aggregation of tropical tree species into functional types and the application on Sabah's dipterocarp lowland rain forests. J. Trop. Ecol. 16, 591–602.

Köhler, P., Ditzer, T., Ong, R.C., Huth, A., 2001. Comparison of measured and modelled growth on permanent plots in Sabahs rain forests. For. Ecol. Manage. 144, 101–111.

Köhler, P., Huth, A., 1998. The effects of tree species grouping in tropical rainforest modelling: simulations with the individual-based model FORMIND. Ecol. Modell. 109, 301–321.

Köhler, P., Huth, A., 2004. Simulating growth dynamics in a South–East Asian rainforest threatened by recruitment shortage and tree harvesting. Clim. Change 67, 95–117.

Köhler, P., Huth, A., 2007. Impacts of recruitment limitation and canopy disturbance on tropical tree species richness. Ecol. Modell. 203, 511–517.

Köhler, P., Huth, A., 2010. Towards ground-truthing of spaceborne estimates of above-ground life biomass and leaf area index in tropical rain forests. Biogeosciences 7, 2531–2543.

Laurance, W.F., Camargo, J.L.C., Luizao, R.C.C., Laurance, S.G., Pimm, S.L., Bruna, E.M., Stouffer, P.C., Williamson, G.B., itez-Malvido, J., Vasconcelos, H.L., van Houtan, K.S., Zartman, C.E., Boyle, S.A., Didham, R.K., Andrade, A., Lovejoy, T.E., 2011. The fate of Amazonian forest fragments: a 32-year investigation. Biol. Conserv. 144, 56–67.

Laurance, W.F., Ferreira, L.V., Rankin-de Merona, J.M., Laurance, S.G., 1998. Rain forest fragmentation and the dynamics of Amazonian tree communities. Ecology 79, 2032–2040.

Laurance, W.F., Lovejoy, T.E., Vasconcelos, H.L., Bruna, E.M., Didham, R.K., Stouffer, P.C., Gascon, C., Bierregaard, R.O., Laurance, S.G., Sampaio, E., 2002. Ecosystem decay of Amazonian forest fragments: a 22-year investigation. Conserv. Biol. 16, 605–618.

Lawton, J.H., Bignell, D.E., Bolton, B., Bloemers, G.F., Eggleton, P., Hammond, P.M., Hodda, M., Holt, R.D., Larsen, T.B., Mawdsley, N.A., Stork, N.E., Srivastava, D.S., Watt, A.D., 1998. Biodiversity inventories, indicator taxa and effects of habitat modification in tropical forest. Nature 391, 72–76.

Le Quéré, C., Moriarty, R., Andrew, R.M., Peters, G.P., Ciais, P., Friedlingstein, P., Jones, S.D., Sitch, S., Tans, P., Arneth, A., Boden, T.A., Bopp, L., Bozec, Y., Canadell, J.G., Chevallier, F., Cosca, C.E., Harris, I., Hoppema, M., Houghton, R.A., House, J.I., Jain, A., Johannessen, T., Kato, E., Keeling, R.F., Kitidis, V., Klein Goldewijk, K., Koven, C., Landa, C.S., Landschützer, P., Lenton, A., Lima, I.D., Marland, G., Mathis, J.T., Metzl, N., Nojiri, Y., Olsen, A., Ono, T., Peters, W., Pfeil, B., Poulter, B., Raupach, M.R., Regnier, P., Rödenbeck, C., Saito, S., Salisbury, J.E., Schuster, U., Schwinger, J., Séférian, R., Segschneider, J., Steinhoff, T., Stocker, B.D., Sutton, A.J., Takahashi, T., Tilbrook, B., van der Werf, G.R., Viovy, N., Wang, Y.P., Wanninkhof, R., Wiltshire, A., Zeng, N., 2015. Global carbon budget 2014. Earth Syst. Sci. Data 7, 47–85.

Lefsky, M.A., Cohen, W.B., Harding, D.J., Parker, G.G., Acker, S.A., Gower, S.T., 2002. Lidar remote sensing of above-ground biomass in three biomes. Global Ecol. Biogeogr. 11, 393–399.

Lehmann, S., Huth, A., 2015. Fast calibration of a dynamic vegetation model with minimum observation data. Ecol. Modell. 301, 98–105.

Meyer, V., Saatchi, S.S., Chave, J., Dalling, J.W., Bohlman, S., Fricker, G.A., Robinson, C., Neumann, M., Hubbell, S., 2013. Detecting tropical forest biomass dynamics from repeated airborne lidar measurements. Biogeosciences 10, 5421–5438.

Morin, X., Fahse, L., Scherer-Lorenzen, M., Bugmann, H., 2011. Tree species richness promotes productivity in temperate forests through strong complementarity between species. Ecol. Lett. 14, 1211–1219.

Morton, D.C., Nagol, J., Carabajal, C.C., Rosette, J., Palace, M., Cook, B.D., Vermote, E.F., Harding, D.J., North, P.R.J., 2014. Amazon forests maintain consistent canopy structure and greenness during the dry season. Nature 506, 221–224.

Moser jr., J.W., 1980. Historical chapters in the development of modern forest growth and yield theory. In: Brown, K.M., Clarke, F.R. (Eds.), Forecasting Forest Stand Dynamics. School of Forestry, Lakehead University, Thunder Bay, ON, pp. 42–61.

Myers, N., Mittermeier, R.A., Mittermeier, C.G., da Fonseca, G.A.B., Kent, J., 2000. Biodiversity hotspots for conservation priorities. Nature 403, 853–858.

Palace, M.W., Sullivan, F.B., Ducey, M.J., Treuhaft, R.N., Herrick, C., Shimbo, J.Z., Mota-E-Silva, J., 2015. Estimating forest structure in a tropical forest using field measurements, a synthetic model and discrete return lidar data. Remote Sens. Environ. 161, 1–11.

Phillips, O.L., Gentry, A.H., 1994. Increasing turnover through time in tropical forests. Science 263, 954–958.

Picard, N., Franc, A., 2003. Are ecological groups of species optimal for forest dynamics modelling? Ecol. Modell. 163, 175–186.

Picard, N., Köhler, P., Mortier, F., Gourlet-Fleury, S., 2012. A comparison of five classifications of species into functional groups in tropical forests of French Guiana. Ecol. Complex. 11, 75–83.

Pimm, S.L., Jenkins, C.N., Abell, R., Brooks, T.M., Gittleman, J.L., Joppa, L.N., Raven, P.H., Roberts, C.M., Sexton, J.O., 2014. The biodiversity of species and their rates of extinction, distribution, and protection. Science 344, 987.

Prentice, I.C., Leemans, R., 1990. Pattern and process and the dynamics of forest structure: a simulation approach. J. Ecol. 78, 340–355.

Prentice, I.C., Sykes, M.T., Cramer, W., 1993. A simulation model for the transient effects of climate change on forest. landscapes. Ecol. Modell. 65, 51–70.

Pretzsch, H., 2009. Forest Dynamics, Growth and Yield. Springer, Berlin, pp. 664.

Pütz, S., Groeneveld, J., Alves, L.F., Metzger, J.P., Huth, A., 2011. Fragmentation drives tropical forest fragments to early successional states: a modelling study for Brazilian Atlantic forests. Ecol. Modell. 222, 1986–1997.

Pütz, S., Groeneveld, J., Henle, K., Knogge, C., Martensen, A.C., Metz, M., Metzger, J.P., Ribeiro, M.C., Dantas de Paula, M., Huth, A., 2014. Long-term carbon loss in fragmented neotropical forests. Nat. Commun. 5, art. 5037.

Ribeiro, M.C., Metzger, J.P., Martensen, A.C., Ponzoni, F.J., Hirota, M.M., 2009. The Brazilian Atlantic Forest: how much is left, and how is the remaining forest distributed? Implications for conservation. Biol. Conserv. 142, 1141–1153.

Rüger, N., Gutiérrez, A.G., Kissling, W.D., Armesto, J.J., Huth, A., 2007. Ecological impacts of different harvesting scenarios for temperate evergreen rain forest in southern Chile—a simulation experiment. For. Ecol. Manage. 252, 52–66.

Rüger, N., Williams-Linera, G., Kissling, W.D., Huth, A., 2008. Long-term impacts of fuelwood extraction on a tropical montane cloud forest. Ecosystems 11, 868–881.

Sato, H., Itoh, A., Kohyama, T., 2007. SEIB-DGVM: a new dynamic global vegetation model using a spatially explicit individual-based approach. Ecol. Modell. 200, 279–307.

Schumacher, S., 2004. The Role of Large-Scale Disturbances and Climate for the Dynamics of Forested Landscapes in the European Alps. Swiss Federal Institute of Technology Zurich, Switzerland, pp. 149.

Schumacher, S., Bugmann, H., Mladenoff, D.J., 2004. Improving the formulation of tree growth and succession in a spatially explicit landscape model. Ecol. Modell. 180, 175–194.

Shugart, H.H., 1984. A Theory of Forest Dynamics. The Blackburn Press, New York, pp. 278.

Shugart, H.H., 1998. Terrestrial Ecosystems in Changing Environments. Cambridge University Press, Cambridge, pp. 537.

Shugart, H.H., 2003. A Theory of Forest Dynamics. The Blackburn Press, New York pp. 278.

Shugart, H.H., Asner, G.P., Fischer, R., Huth, A., Knapp, N., Le Toan, T., Shuman, J.K., 2015. Computer and remote-sensing infrastructure to enhance large-scale testing of individual-based forest models. Front Ecol. Environ. 13, 503–511.

Shugart, H.H., West, D.C., 1977. Development of an Appalachian deciduous forest succession model and its application to assessment of the impact of the chestnut blight. J. Environ. Manage. 5, 161–179.

Sitch, S., Smith, B., Prentice, I.C., Arneth, A., Bondeau, A., Cramer, W., Kaplan, J.O., Levis, S., Lucht, W., Sykes, M.T., Thonicke, K., Venevsky, S., 2003. Evaluation of ecosystem dynamics, plant geography and terrestrial carbon cycling in the LPJ dynamic global vegetation model. Global Change Biol. 9, 161–185.

Skole, D., Tucker, C., 1993. Tropical deforestation and habitat fragmentation in the Amazon: satellite data from 1978 to 1988. Science 260, 1905–1910.

Slik, J.W.F., Arroyo-Rodríguez, V., Aiba, S.-I., Alvarez-Loayza, P., Alves, L.F., Ashton, P., Balvanera, P., Bastian, M.L., Bellingham, P.J., van den Berg, E., Bernacci, L., da Conceição Bispo, P., Blanc, L., Böhning-Gaese, K., Boeckx, P., Bongers, F., Boyle, B., Bradford, M., Brearley, F.Q., Breuer-Ndoundou Hockemba, M., Bunyavejchewin, S., Calderado Leal Matos, D., Castillo-Santiago, M., Catharino, E.L.M., Chai, S.-L., Chen, Y., Colwell, R.K., Chazdon, R.L., Clark, C., Clark, D.B., Clark, D.A., Culmsee, H., Damas, K., Dattaraja, H.S., Dauby, G., Davidar, P., Dewalt, S.J., Doucet, J.-L., Duque, A., Durigan, G., Eichhorn, K.A.O., Eisenlohr, P.V., Eler, E., Ewango, C., Farwig, N., Feeley, K.J., Ferreira, L., Field, R., de Oliveira Filho, A.T., Fletcher, C., Forshed, O., Franco, G., Fredriksson, G., Gillespie, T., Gillet, J.F., Amarnath, G., Griffith, D.M., Grogan, J., Gunatilleke, N., Harris, D., Harrison, R., Hector, A., Homeier, J., Imai, N., Itoh, A., Jansen, P.A., Joly, C.A., de Jong, B.H.J., Kartawinata, K., Kearsley, E., Kelly, D.L., Kenfack, D., Kessler, M., Kitayama, K., Kooyman, R., Larney, E., Laumonier, Y., Laurance, S., Laurance, W.F., Lawes, M.J., Leao do Amaral, I., Letcher, S.G., Lindsell, J., Lu, X., Mansor, A., Marjokorpi, A., Martin, E.H., Meilby, H., Melo, F.P.L., Metcalfe, D.J., Medjibe, V.P., Metzger, J.P., Millet, J., Mohandass, D., Montero, J.C., de Morisson Valeriano, M., Mugerwa, B., Nagamasu, H., Nilus, R., Ochoa-Gaona, S., Page, O.N., Parolin, P., Parren, M., Parthasarathy, N., Paudel, E., Permana, A., Piedade, M.T.F., Pitman, N.C.A., Poorter, L., Poulsen, A.D., Poulsen, J., Powers, J., Prasad, R.C., Pyravaud, J.P., Razafimahaimodison, J.C., Reitsma, J., dos Santos, J.R., Spironello, W.R., Romero-Saltos, H., Rovero, F., Rozak, A.H., Ruokolainen, K., Rutishauser, E., Saitert, F., Saner, P., Santos, B.A., Santos, F., Sarker, S.K., Satdichanha, M., Schmitt, C.B., Schöngart, J., Schulze, M., Suganuma, M.S., Sheil, D., da Silva Pinheiro, E., Sist, P., Stevart, T., Sukumar, R., Sun, I.-F., Sunderland, T., Suresh, H.S., Suzuki, E., Tabarelli, M., Tang, J., Targhetta, N., Theilade, I., Thomas, D.W., Tchouto, P., Hurtado, J., Valencia, R., van Valkenburg, J.L.C.H., Van Do, T., Vasquez, R., Verbeeck, H., Adekunle, V., Vieira, S.A., Webb, C.O., Whitfeld, T., Wich, S.A., Williams, J., Wittmann, F., Wöll, J., Yang, X., Yao, C.Y.A., Yap, S.L., Yoneda, T., Zahawi, R.A., Zakaria, R., Zang, R., de Assis, R.L., Garcia Luize, B., Venticinque, E.M., 2015. An estimate of the number of tropical tree species. Proc. Natl. Acad. Sci. U.S.A. 112, 7472–7477.

Smith, T.M., Shugart, H.H., 1997. Plant Functional Types. In Their Relevance to Ecosystem Properties and Global Change. Cambridge University Press, Cambridge.

Snell, R.S., Huth, A., Nabel, J.E.M.S., Bocedi, G., Travis, J.M.J., Gravel, D., Bugmann, H., Gutiérrez, A.G., Hickler, T., Higgins, S.I., Reineking, B., Scherstjanoi, M., Zurbriggen, N., Lischke, H., 2014. Using dynamic vegetation models to simulate plant range shifts. Ecography 37, 1184–1197.

Taubert, F., Frank, K., Huth, A., 2012. A review of grassland models in the biofuel context. Ecol. Modell. 245, 84–93.

Thornley, J.H.M., Johnson, I.R., 1990. Plant and Crop Modelling. Claredon Press Oxford.

Ticktin, T., 2004. The ecological implications of harvesting non-timber forest products. J. Appl. Ecol. 41, 11–21, 1990.

Tietjen, B., Huth, A., 2006. Modelling dynamics of managed tropical rainforests—an aggregated approach. Ecol. Modell. 199, 421–432.

Tolson, B.A., Shoemaker, C.A., 2007. Dynamically dimensioned search algorithm for computationally efficient watershed model calibration. Water Resour. Res. 43, 43.

Urban, D.L., Bonan, G.B., Smith, T.M., Shugart, H.H., 1991. Spatial applications of gap models. For. Ecol. Manage. 42, 95–110.

Vilà, M., Vayreda, J., Comas, L., Ibanez, J.J., Mata, T., Obon, B., 2007. Species richness and wood production: a positive association in Mediterranean forests. Ecol. Lett. 10, 241–250.

Wang, X.H., Piao, S.L., Ciais, P., Friedlingstein, P., Myneni, R.B., Cox, P., Heimann, M., Miller, J., Peng, S.S., Wang, T., Yang, H., Chen, A.P., 2014. A two-fold increase of carbon cycle sensitivity to tropical temperature variations. Nature 506, 212-+.

Wårlind, D., Smith, B., Hickler, T., Arneth, A., 2014. Nitrogen feedbacks increase future terrestrial ecosystem carbon uptake in an individual-based dynamic vegetation model. Biogeosciences 11, 6131–6146.

Whitmore, T.C., 1998. An Introduction to Tropical Rain Forests. Oxford University Press, Oxford, pp. 296.

Yan, X.D., Shugart, H.H., 2005. FAREAST: a forest gap model to simulate dynamics and patterns of eastern Eurasian forests. J. Biogeogr. 32, 1641–1658.

Zhang, Y., Chen, H.Y.H., Reich, P.B., 2012. Forest productivity increases with evenness, species richness and trait variation: a global meta-analysis. J. Ecol. 100, 742–749.

Appendix A

Overview of publications related to the FORMIND forest model family. Publications are ordered by research field as shown in Figure 6. The column 'module added' indicates the first appearance of a new submodule in the forest model. 'Additional applications' include FORMIND model versions developed for temperate forests and grasslands. Publications of the related FORMIX model are shown in italics. An updated list can be found at http://formind.org/publications/.

Research Field	Publication	Specific Research Topic	Region + Forest Type	Module Added
Grouping of species (PFT)	Köhler and Huth (1998)	The effects of tree species grouping in tropical rainforest modelling: Simulations with the individual-based model FORMIND	Malaysia, tropical forest	FORMIND
	Köhler et al. (2000)	Concepts for the aggregation of tropical tree species into functional types and the application on Sabah's dipterocarp lowland rain forests	Malaysia, tropical forest	
	Picard et al. (2012)	A comparison of five classifications of species into functional groups in tropical forests of French Guiana	French Guiana, tropical forest	
	Kazmierczak et al. (2014)	A neutral vs. non-neutral parametrizations of a physiological forest gap model	Panama, tropical forest	
Logging	*Ditzer et al. (2000)*	*The process-based stand growth model Formix 3-Q applied in a GIS environment for growth and yield analysis in a tropical rain forest*	*Malaysia, tropical forest*	
	Huth and Ditzer (2001)	*Long-term impacts of logging in a tropical rain forest - a simulation study*	*Malaysia, tropical forest*	*Logging*
	Kammesheidt et al. (2001)	Sustainable timber harvesting in Venezuela: a modelling approach	Venezuela, tropical forest	Logging
	Kammesheidt et al. (2002)	*Simulating logging scenarios in secondary forest embedded in a fragmented neotropical landscape*	*Paraguay, tropical forest*	
	Glauner et al. (2003)	*Growth and yield of tropical moist forest for forest planning: an inquiry through modeling*	*Malaysia, tropical forest*	
	Köhler and Huth (2004)	Simulating growth dynamics in a South-East Asian rainforest threatened by recruitment shortage and tree harvesting	Malaysia, tropical forest	
	Huth et al. (2004)	Multicriteria evaluation of simulated logging scenarios in a tropical rain forest	Malaysia, tropical forest	
	Huth et al. (2005)	Using multicriteria decision analysis and a forest growth model to assess impacts of tree harvesting in Dipterocarp lowland rain forests	Malaysia, tropical forest	

Research Field	Publication	Specific Research Topic	Region + Forest Type	Module Added
	Tietjen and Huth (2006)	*Modelling dynamics of managed tropical rainforests - an aggregated approach*	*Malaysia, tropical forest*	
	Rüger et al. (2007)	Ecological impacts of different harvesting scenarios for temperate evergreen rain forest in southern Chile - A simulation experiment	Chile, temperate rain forest	
	Rüger et al. (2008)	Long-term impacts of fuelwood extraction on a tropical montane cloud forest	Mexico, tropical montane forest	
Fragmentation	Köhler et al. (2003)	Simulating the long-term response of tropical wet forests to fragmentation	French Guiana, tropical wet forests	Fragmentation
	Groeneveld et al. (2009)	The impact of fragmentation and density regulation on forest succession in the Atlantic rain forest	Brazil, Atlantic Rain Forest	Density regulation
	Pütz et al. (2011)	Fragmentation drives tropical forest fragments to early successional states: A modelling study for Brazilian Atlantic forests	Brazil, Atlantic Rain Forest	
	Pütz et al. (2014)	Long-term carbon loss in fragmented Neotropical forests	Brazil, Atlantic Rain Forest	
	Dantas de Paula et al. (2015)	Tropical forest degradation and recovery in fragmented landscapes - Simulating changes in tree community, forest hydrology and carbon balance	Brazil, Atlantic Rain Forest	
Parametrization	*Bossel and Krieger (1991)*	*Simulation model of natural tropical forest dynamics*	*Malaysia, tropical forest*	*FORMIX*
	Bossel and Krieger (1994)	*Simulation of multi-species tropical forest dynamics using a vertically and horizontally structured model*	*Malaysia, tropical forest*	
	Huth and Ditzer (2000)	*Simulation of the growth of a lowland Dipterocarp rain forest with FORMIX3*	*Malaysia, tropical forest*	
	Köhler et al. (2001)	Comparison of measured and modelled growth on permanent plots in Sabah's rain forests	Malaysia, tropical forest	
	Dislich et al. (2009)	Simulating forest dynamics of a tropical montane forest in South Ecuador	Ecuador, tropical montane forest	
	Hartig et al. (2014)	Approximate Bayesian parameterization of a process-based tropical forest model	Ecuador, tropical forest	
	Lehmann and Huth (2015)	Fast calibration of a dynamic vegetation model with minimum observation data	Panama, tropical forest	
Climate change	Gutiérrez et al. (2014)	Increased drought impacts on temperate rainforests from southern South America: Results of a process-based, dynamic forest model	Chile, Temperate Rainforests	Climate Effects

Research Field	Publication	Specific Research Topic	Region + Forest Type	Module Added
	Fischer et al. (2014)	*Simulating the impacts of reduced rainfall on carbon stocks and net ecosystem exchange in a tropical forest*	*Madagascar, tropical forest*	*Climate Effects*
	Hiltner et al. (2016)	*Impacts of precipitation variability on the dynamics of a dry tropical montane forest*	*Ethiopia, tropical montane forest*	
Biodiversity	Köhler and Huth (2007)	Impacts of recruitment limitation and canopy disturbance on tropical tree species richness	Malaysia, tropical forest	
Remote sensing	Köhler and Huth (2010)	Towards ground-truthing of space-borne estimates of above-ground life biomass and leaf area index in tropical rain forests	Malaysia, tropical forest	
Disturbance	Dislich and Huth (2012)	Modelling the impact of shallow landslides on forest structure in tropical montane forests	Ecuador, tropical montane forest	Landslides
	Gutiérrez and Huth (2012)	Successional stages of primary temperate rainforests of Chiloé Island, Chile	Chile, Temperate Rainforests	Windstorms
Ecosystem carbon balance	Fischer et al. (2015)	Simulating carbon stocks and fluxes of an African tropical montane forest with an individual-based forest model	Tanzania, lower montane tropical forest	Above- and belowground carbon fluxes
Additional applications	Taubert et al. (2012)	Transfer FORMIND to temperate grasslands (GRASMIND). A review of grassland models in the biofuel context	Temperate grasslands	Transfer to Grasslands
	van Oijen et al. (2013)	Bayesian calibration, comparison and averaging of six forest models, using data from Scots pine stands across Europe	Austria, Belgium, Estonia, Finland, Scots pine stands	
	Bohn et al. (2014)	Application of FORMIND in temperate forests in Europe (8 tree species). Of climate and its resulting tree growth: Simulating the productivity of temperate forests	Germany, France, Temperate forest	Climate Effects

References

Bohn, F.J., Frank, K., Huth, A., 2014. Of climate and its resulting tree growth: Simulating the productivity of temperate forests. Ecological Modelling 278, 9-17.

Bossel, H., Krieger, H., 1991. Simulation model of natural tropical forest dynamics. Ecological Modelling 59, 37-71.

Bossel, H., Krieger, H., 1994. Simulation of multi-species tropical forest dynamics using a vertically and horizontally structured model. Forest Ecology and Management 69, 123-144.

Dantas de Paula, M., Groeneveld, J., Huth, A., 2015. Tropical forest degradation and recovery in fragmented landscapes - Simulating changes in tree community, forest hydrology and carbon balance. Global Ecology and Conservation 3, 664-677.

Dislich, C., Günter, S., Homeier, J., Schröder, B., Huth, A., 2009. Simulating forest dynamics of a tropical montane forest in South Ecuador. Erdkunde 63, 347-364.

Dislich, C., Huth, A., 2012. Modelling the impact of shallow landslides on forest structure in tropical montane forests. Ecological Modelling 239, 40-53.

Ditzer, T., Glauner, R., Forster, M., Köhler, P., Huth, A., 2000. The process-based stand growth model Formix 3-Q applied in a GIS environment for growth and yield analysis in a tropical rain forest. Tree Physiology 20, 367-381.

Fischer, R., Armstrong, A., Shugart, H.H., Huth, A., 2014. Simulating the impacts of reduced rainfall on carbon stocks and net ecosystem exchange in a tropical forest. Environmental Modelling & Software 52, 200-206.

Fischer, R., Ensslin, A., Rutten, G., Fischer, M., Schellenberger Costa, D., Kleyer, M., Hemp, A., Paulick, S., Huth, A., 2015. Simulating carbon stocks and fluxes of an African tropical montane forest with an individual-based forest model. PLoS ONE 10, e0123300.

Glauner, R., Ditzer, T., Huth, A., 2003. Growth and yield of tropical moist forest for forest planning: an inquiry through modeling. Canadian Journal of Forest Research-Revue Canadienne de Recherche Forestière 33, 521-535.

Groeneveld, J., Alves, L.F., Bernacci, L.C., Catharino, E.L.M., Knogge, C., Metzger, J.P., Pütz, S., Huth, A., 2009. The impact of fragmentation and density regulation on forest succession in the Atlantic rain forest. Ecological Modelling 220, 2450-2459.

Gutiérrez, A.G., Armesto, J.J., Díaz, M.F., Huth, A., 2014. Increased drought impacts on temperate rainforests from southern South America: Results of a process-based, dynamic forest model. PLoS ONE 9, e103226.

Gutiérrez, A.G., Huth, A., 2012. Successional stages of primary temperate rainforests of Chiloé Island, Chile. Perspectives in Plant Ecology, Evolution and Systematics 14, 243-256.

Hartig, F., Dislich, C., Wiegand, T., Huth, A., 2014. Technical Note: Approximate Bayesian parameterization of a process-based tropical forest model. Biogeosciences 11, 1261-1272.

Hiltner, U., Bräuning, A., Gebrekirstos, A., Huth, A., Fischer, R., 2016. Impacts of precipitation variability on the dynamics of a dry tropical montane forest". Ecological Modelling, 320, 92-101

Huth, A., Ditzer, T., 2000. Simulation of the growth of a lowland Dipterocarp rain forest with FORMIX3. Ecological Modelling 134, 1-25.

Huth, A., Ditzer, T., 2001. Long-term impacts of logging in a tropical rain forest - a simulation study. Forest Ecology and Management 142, 33-51.

Huth, A., Drechsler, M., Köhler, P., 2004. Multicriteria evaluation of simulated logging scenarios in a tropical rain forest. Journal of Environmental Management 71, 321-333.

Huth, A., Drechsler, M., Köhler, P., 2005. Using multicriteria decision analysis and a forest growth model to assess impacts of tree harvesting in Dipterocarp lowland rain forests. Forest Ecology and Management 207, 215-232.

Kammesheidt, L., Köhler, P., Huth, A., 2001. Sustainable timber harvesting in Venezuela: a modelling approach. Journal of Applied Ecology 38, 756-770.

Kammesheidt, L., Köhler, P., Huth, A., 2002. Simulating logging scenarios in secondary forest embedded in a fragmented neotropical landscape. Forest Ecology and Management 170, 89-105.

Kazmierczak, M., Wiegand, T., Huth, A., 2014. A neutral vs. non-neutral parametrizations of a physiological forest gap model. Ecological Modelling 288, 94-102.

Köhler, P., Chave, J., Riéra, B., Huth, A., 2003. Simulating the long-term response of tropical wet forests to fragmentation. Ecosystems 6, 114-128.

Köhler, P., Ditzer, T., Huth, A., 2000. Concepts for the aggregation of tropical tree species into functional types and the application on Sabah's dipterocarp lowland rain forests. Journal of Tropical Ecology 16, 591-602.

Köhler, P., Ditzer, T., Ong, R.C., Huth, A., 2001. Comparison of measured and modelled growth on permanent plots in Sabahs rain forests. Forest Ecology and Management 144, 101-111.

Köhler, P., Huth, A., 1998. The effects of tree species grouping in tropical rainforest modelling: Simulations with the individual-based model FORMIND. Ecological Modelling 109, 301-321.

Köhler, P., Huth, A., 2004. Simulating growth dynamics in a South-East Asian rainforest threatened by recruitment shortage and tree harvesting. Climatic Change 67, 95-117.

Köhler, P., Huth, A., 2007. Impacts of recruitment limitation and canopy disturbance on tropical tree species richness. Ecological Modelling 203, 511-517.

Köhler, P., Huth, A., 2010. Towards ground-truthing of spaceborne estimates of above-ground life biomass and leaf area index in tropical rain forests. Biogeosciences 7, 2531-2543.

Lehmann, S., Huth, A., 2015. Fast calibration of a dynamic vegetation model with minimum observation data. Ecological Modelling 301, 98-105.

Picard, N., Köhler, P., Mortier, F., Gourlet-Fleury, S., 2012. A comparison of five classifications of species into functional groups in tropical forests of French Guiana. Ecological Complexity 11, 75-83.

Pütz, S., Groeneveld, J., Alves, L.F., Metzger, J.P., Huth, A., 2011. Fragmentation drives tropical forest fragments to early successional states: A modelling study for Brazilian Atlantic forests. Ecological Modelling 222, 1986-1997.

Pütz, S., Groeneveld, J., Henle, K., Knogge, C., Martensen, A.C., Metz, M., Metzger, J.P., Ribeiro, M.C., Dantas de Paula, M., Huth, A., 2014. Long-term carbon loss in fragmented Neotropical forests. Nature Communications 5, art. 5037.

Rüger, N., Gutiérrez, A.G., Kissling, W.D., Armesto, J.J., Huth, A., 2007. Ecological impacts of different harvesting scenarios for temperate evergreen rain forest in southern Chile - A simulation experiment. Forest Ecology and Management 252, 52-66.

Rüger, N., Williams-Linera, G., Kissling, W.D., Huth, A., 2008. Long-term impacts of fuelwood extraction on a tropical montane cloud forest. Ecosystems 11, 868-881.

Taubert, F., Frank, K., Huth, A., 2012. A review of grassland models in the biofuel context. Ecological Modelling 245, 84-93.

Tietjen, B., Huth, A., 2006. Modelling dynamics of managed tropical rainforests - an aggregated approach. Ecological Modelling 199, 421-432.

van Oijen, M., Reyer, C., Bohn, F.J., Cameron, D.R., Deckmyn, G., Flechsig, M., Härkönen, S., Hartig, F., Huth, A., Kiviste, A., Lasch, P., Mäkelä, A., Mette, T., Minunno, F., Rammer, W., 2013. Bayesian calibration, comparison and averaging of six forest models, using data from Scots pine stands across Europe. Forest Ecology and Management 289, 255-268.

Appendix B General concept of FORMIND

FORMIND 3.0 is an individual- and process-based model designed for simulating forest dynamics. The model is applied to various forest sites all over the world facing different challenges of forest ecology during the last decades.
This document introduces the most frequendly used approaches of the entire range of different model versions, which can be currently applied (a full description can be found at www.formind.org).

In FORMIND 3.0 vegetation is simulated on an area of size A_{area}, which is a composite of regularly ordered, quadratic patches of size A_{patch} [m^2] described by their location within the area (Fig. 1). Individual trees grow within the patches, but do not have spatially explicit positions within a patch (the gap model approach).

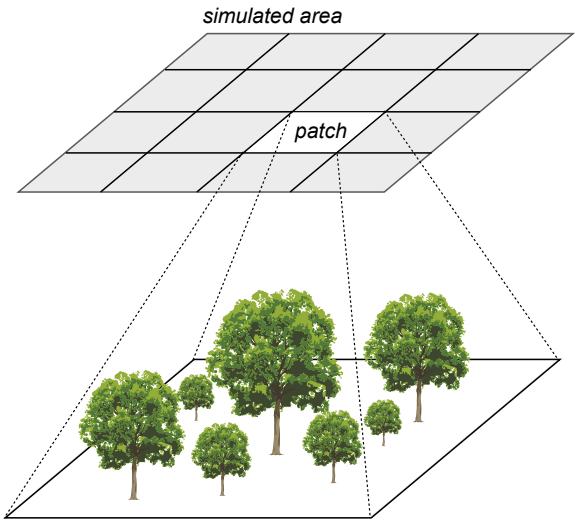

Figure 1: *Illustration of the simulated area and its composition of regularly ordered patches. Individual trees do not have spatially explicit positions within the patches. Only for an illustrative purpose, we show positioned trees on an exemplary patch.*

The trees change their size during the simulation according to a set of ecophysiological and morphological parameters used within the modelled processes. The modelled processes are simulated on different levels: (i) area-level, (ii) patch-level or (iii) on the level of a single tree .

- Appendix C - **Geometry**
  trees are described by several geometric relationships. tree types (in some projects

we use the concept of plant functional types in others real species) can differ in their parameter sets of these relationships.

Within each time step Δt (e.g. one year), the following main processes can be calculated:

- Appendix D - **Recruitment and establishment**
  Establishment of recruited seeds is modelled on the patch-level, whereby the distribution of seeds is simulated on the area-level.

- Appendix E - **Mortality**
  First, an event-driven mortality due to crowding can take place on the patch-level. Afterwards, mortality rates affects each trees (e.g. base mortality). Finally, every dying tree has a change to fall down and damage other trees .

- Appendix F - **Environment**
  The patches of the simulation area are homogeneously concerning climatic input variables. Based on these input parameters, the environment of the trees is specified. For example, the radiation above canopy and day length are equal for all patches. The vertical attenuation of the incoming radiation (i.e. light climate) is calculated for each patch based on the vegetation state, so that light intensity at different heights can differ between patches dependent on the number of trees shading each other. Reduced light availability result in a reduced gross photosynthesis of a tree . Limited soil water resources can also reduce the gross photosynthesis of an individual. In the same manner as the light climate, soil water contents can differ between patches during the simulation, although the initial soil water content and other soil properties (e.g. soil porosity) are equal for all patches. Differences in soil water content between patches are dependent on the number of trees per patch, which take up soil water resources. Further, type-specific effect of air temperature can also limit gross photosynthesis and affect respiration of an individual.

- Appendix G - **Growth**
  The growth of a single tree is determined by its gross productivity, respiration and type-specific morphological parameters. Respiration is calculated on the level of an individual. An increase in biomass per tree is modelled as the difference between gross photosynthesis and respiration. The allocation of the resulting biomass increase (including the increase of geometrical properties according to Appendix C) act on the level of a tree .

- Appendix H - **Disturbances**
  Fire and landslide events are simulated on the area-level.

- Appendix I **- Carbon cycle**
  Carbon stocks and carbon fluxes were calculated on the area-level. For the investigation of the forest carbon balance a simple compartment approach was implemented.

- Appendix J **- Logging**
  Selective logging of trees is simulated on the area-level. The selection is based on tree - specific characteristics (e.g. stem diameter or tree type) and represent conventional or reduced impact logging.

The modelled processes, which are summarized within the above mentioned main processes, are scheduled in a serial way. For an overview on the modelled processes and their schedule see Fig. 2.

Periodic or open boundary conditions can be used. For periodic boundary conditions, that means processes leaving one side of the simulation area are entering the area on the opposite side again. For open boundary conditions, that means processes leaving the simulation area are lost. No migration entering the open boundaries would be considered.

For the purpose of calculations within the processes of light climate and crowding mortality, the above-ground space is discretized into vertical height layers of constant width Δh. Table 1 shows general input parameters.

Table 1: *Parameters describing space and time.*

Description	Parameter	values range	Unit
Time step	Δt	$365^{-1} - 5$	year
Simulation area	A_{area}	1-400	hectare
Patch area	A_{patch}	400	m^2
Width of height layers h	Δ	0.5	m

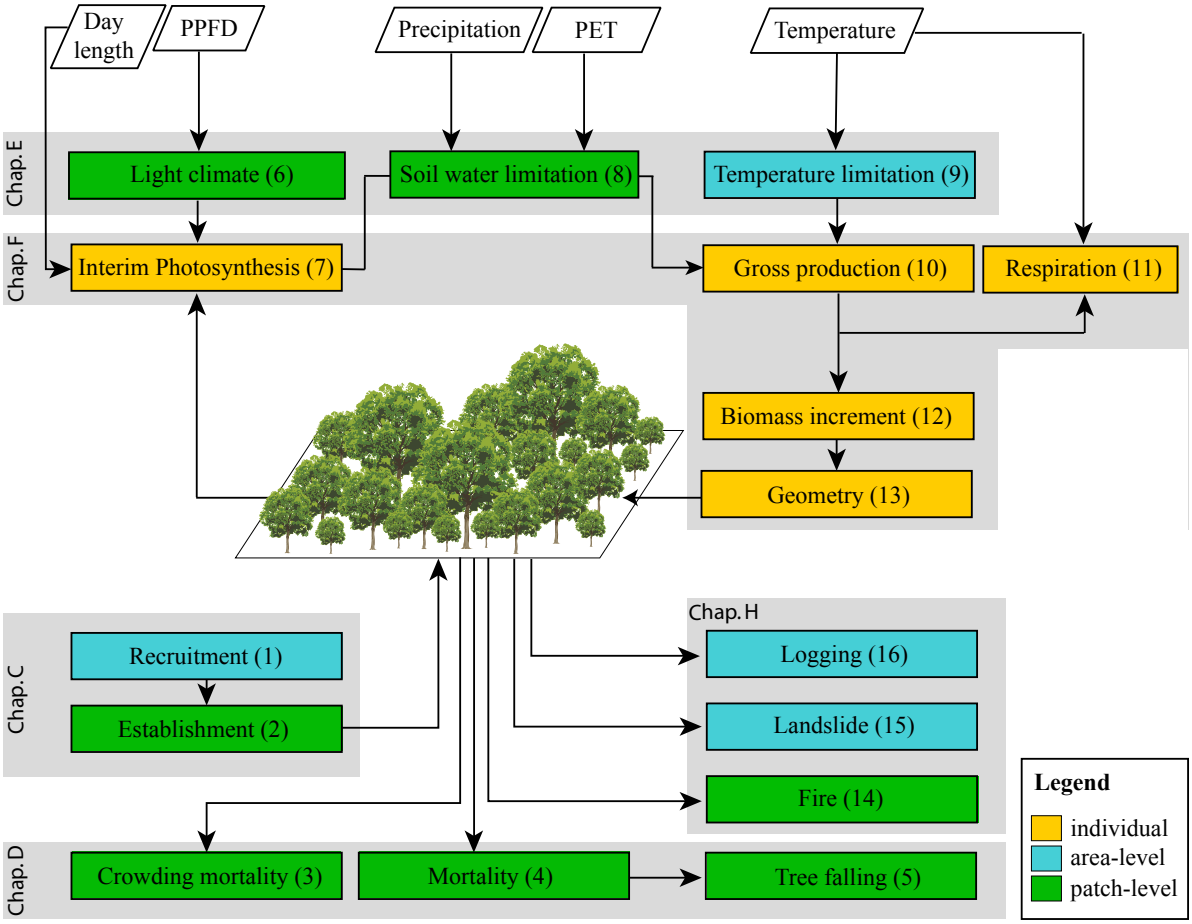

Figure 2: *Block diagram of the modelled processes. Different colours indicate the spatial scale on which each process is calculated (blue = area, green = patch, orange= individual). Italic written boxes show processes which are simulated with time steps of higher resolution than* Δt *(e.g one year). Numbers in brackets within each box show the serial order of their calculation within one time step* Δt*. Grey frames that underly these boxes group them according to the above mentioned main processes and their corresponding chapters. Rhombuses indicate climatic input parameters with the following abbreviations: PET – potential evapotranspiration, PPFD – photoactive photon flux density.*

Appendix C Geometry

Although individual trees in real forests do not necessarily have identical shapes, we model each tree by a cylindrical stem and a cylindrical crown (Fig. 3). The geometry of an individual can be described completely by the following size characteristics: stem diameter (D), height (H), crown diameter (C_D), crown length (C_L) and crown projection area (C_A) as shown in Fig. 3.

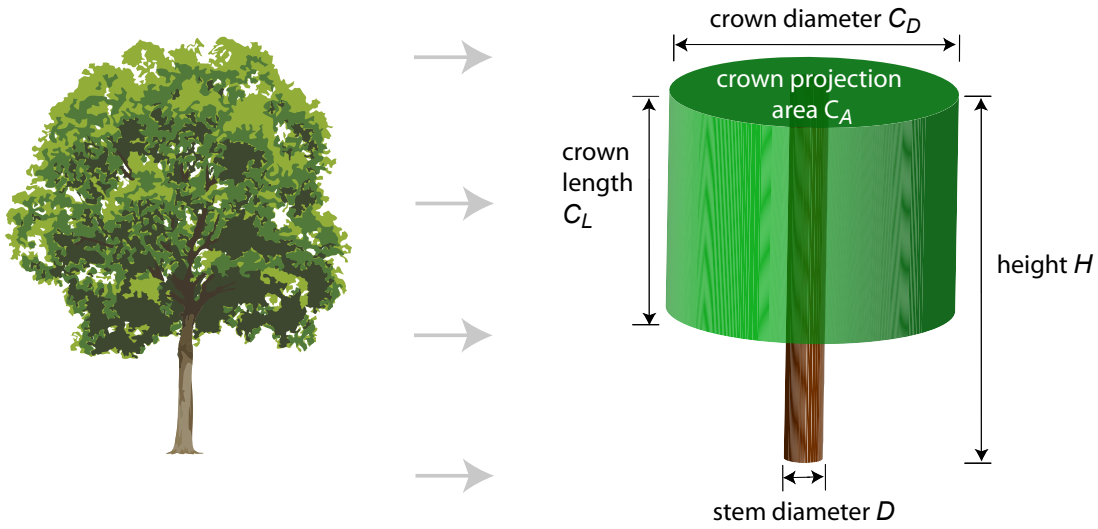

Figure 3: *Geometrical representation of a single tree . The following abbreviations describe size characteristics of the modelled tree geometry: D - stem diameter, H - height, C_D - crown diameter, C_L - crown length, C_A crown projection area.*

These size characteristics are functionally related to each other. In the following, we describe the functional relationships that can be used. Parameters of the described relationships can vary between different tree types. Some graphical examples are given in Fig. 3. FORMIND offers also other relationships as the most used ones, which are described below. If you are interested in the optional relationships, see www.formind.org.

C.1 Height - Stem Diameter - Relationship

The height H [m] of a tree relates to its stem diameter D [cm] by:

$$H = h_0 \cdot D^{h_1}, \tag{1}$$

where h_0 and h_1 are type-specific parameters.

C.2 Crown length - Height - Relationship

The crown length C_L [m] of a tree is modelled as a fraction of its height H [m]:

$$C_L = c_{l0} \cdot H, \tag{2}$$

where c_{l0} is a type-specific parameter.

C.3 Crown diameter - Stem diameter - Relationship

The second dimension of the cylindrical crown, i.e. the crown diameter C_D [m] of a tree relates to its stem diameter D [cm] by:

$$C_D = c_{d0} \cdot D^{c_{d1}} - c_{d2}, \tag{3}$$

where c_{d0}, c_{d1} and c_{d2} are type-specific parameters.

C.4 Crown area - Crown diameter - Relationship

The crown projection area C_A [m^2] of a tree is simply the ground area of the modelled cylindrical crown:

$$C_A = \frac{\pi}{4} \cdot C_D^2. \tag{4}$$

C.5 Aboveground biomass - Stem diameter - Relationship

The aboveground volume of a tree captures biomass (i.e. organic dry matter). The following different ways of modelling the aboveground biomass are included in FORMIND 3.0 :

Geometrical approach (most frequently used)

Aboveground biomass B [t_{ODM}] of a tree is calculated in relation to its stem diameter D [m] and height H [m] by:

$$B = \frac{\pi}{4} \cdot D^2 \cdot H \cdot f \cdot \frac{\rho}{\sigma}, \tag{5}$$

whereby the calculation simply represents the volume of the tree stem (according to its geometry) multiplied by three factors, which describe the biomass content more concisely.

Firstly, f [-] denotes a type-specific form factor, which accounts for deviations of the stem from a cylindrical shape. Secondly, the parameter ρ [t_{ODM}/m^3] represents the wood density, which describes how much organic dry matter per unit of volume the stem contains. Thirdly, the division by the parameter σ [t_{ODM}/t_{ODM}], which represents the fraction of total aboveground biomass attributed to the stem, results then in the total aboveground biomass B.

In contrast to the constant parameters ρ and σ, the form factor f can change during the growth of an individual with respect to its stem diameter D [cm] by using either:

- $$f = f_0 \cdot exp\left(f_1 \cdot D^{f_2}\right), \tag{6}$$
  whereby f_0, f_1 and f_2 are type-specific parameters or
- $$f = f_0 \cdot D^{f_1}, \tag{7}$$
  whereby f_0 and f_1 are type-specific parameters.

C.6 Leaf area index - Stem diameter - Relationship

In general, aboveground biomass is divided between woody biomass captured in the stem and green biomass captured in the crown leaves. Important for the photosynthetic production of a tree is the green biomass captured in crown leaves. As leaves absorb radiation for photosynthesis, the total amount of one-sided leaf area per unit of crown projection area (i.e. the individual's leaf area index) is of main interest. The leaf area index LAI [$\mathrm{m}^2/\mathrm{m}^2$] of a tree relates functionally to its stem diameter D [cm] by:

$$LAI = l_0 \cdot D^{l_1}, \tag{8}$$

whereby l_0 and l_1 are type-specific parameters.

All parameters mentioned above are listed in Tab.4.

C.7 Maximum Values

The trees cannot grow indefinitely in FORMIND 3.0 . We introduce the following maximum values for a plausible geometry of a mature individual:

Table 2: *Summary of the morphological parameter range based on tropical parameterizations.*

parameter	values range	unit
$H_{\max}$	15 - 55	m
h_0	2 - 7	-
h_1	0.2 - 0.7	-
c_{l0}	0.3 - 0.4	-
c_{d0}	0.5 - 0.6	-
c_{d1}	0.65 - 0.75	-
c_{d2}	0.0 - 0.3	-
ρ	0.4 - 0.8	$\frac{todm}{m^3}$
σ	0.7	$\frac{todm}{todm}$
f_0	0.75 - 0.80	-
f_1	-0.15 - -0.20	-
l_0	1 - 3	-
l_1	0.1 - 0.3	-

- maximum stem diameter D_{max} [m]
- maximum height H_{max} [m]

Either the maximum stem diameter or the maximum height is given as a type-specific input parameter. The missing maximum value and the corresponding maximum biomass B_{max} $[t_{ODM}]$ are then derived using the functional relationships mentioned in section C.1 and section C.5. The maximum values are used in Appendix G.

Appendix D Recruitment and Establishment

FORMIND 3.0 includes two different possibilities to model recruitment:

- by using global constant in-growth rates or
- by seed production and dispersal of mother trees.

D.1 Global in-growth rates

The number of recruited seeds is assumed to be brought into the local community from an intact forest community surrounding the simulated area. This number N_{seed} [$^1/_{\text{yr ha}}$] is thereby a constant type-specific parameter independent of the density of individuals already existing on the simulated area.

The recruited seeds directly enter the seed pool, but they may only germinate and establish in the next time step. Each patch is assigned an own seed pool. The recruited seeds are distributed uniformly across the patches and added to the corresponding seed pool in an amount of:

$$N_{pool} = \left\lfloor \frac{N_{seed}}{\#patches} \right\rfloor . \tag{9}$$

If the number of ingrowing seeds N_{seed} is not a multiple of the number of patches $\#patches$, a certain number of seeds will remain which are distributed randomly to the patches. For this, the patches are considered one by one incrementally starting with the first. Within each considered patch and for each remaining seed, which has not been distributed yet, its probability of assignment to the currently considered patch is compared with a random number (uniformly distributed in [0;1]). In the case of successful assignment (i.e. random number $\leq 1/\#patches$), the seed number per patch N_{pool} is incremented and the number of remaining seeds decremented. At the end, the last patch receives all remaining seeds.

Before the start of the simulation, N_{init} seeds already existing in the seed pool per patch (i.e. $N_{pool} = N_{init}$) can be defined for each type, which may germinate and establish as seedlings already in the first time step.

D.2 Seed production and dispersal of mother trees

Before the start of the simulation, it is obligatory to assign to the seed pool of each patch a type-specific number of seeds N_{init}.

During the simulation, each individual of a cohort per patch is able to produce a predefined type-specific number of seeds N_{seed} on its own as a mother plant if it reaches a predefined stem diameter D_{rep}. These produced seeds are dispersed among the neighboring patches surrounding that patch the mother plant is located in. The dispersal is dependent on a defined dispersal kernel, the crown diameter C_D of the mother plant and a predefined type-specific average dispersal distance $dist$.

There is no distinction between different dispersal agents (e.g. wind, birds, mammals). The dispersal kernel is assumed to be Weibull distributed with a shape parameter of 2 and a scale parameter of $(dist + C_D/2)^2$. Presuming rotation symmetry, the probability density f_{disp} that seeds are dispersed at a distance r from the mother plant is defined as:

$$f_{disp}(r) = \frac{2 \cdot r}{\left(dist + \frac{C_D}{2}\right)^2} \cdot e^{-\frac{r^2}{\left(dist + \frac{C_D}{2}\right)^2}}. \tag{10}$$

For each seed per mother plant per patch, a distance r is stochastically drawn from the dispersal kernel $f_{disp}(r)$. Using the calculated distance r and a random direction DIR (drawn from a uniform distribution in the range of [0°;360°]), the target coordinates of the dispersed seed are determined in the following way:

$$x_{seed} = x_{ind} + r \ sin\left(2 \ \pi \ \frac{DIR}{360}\right) \tag{11}$$

$$y_{seed} = y_{ind} + r \ cos\left(2 \ \pi \ \frac{DIR}{360}\right) \tag{12}$$

whereby (x_{ind}, y_{ind}) is a randomly generated position of the mother plant within its corresponding patch and (x_{seed}, y_{seed}) is the calculated virtual position of the dispersed seed on the simulation area. As in FORMIND 3.0 individuals do not have spatially explicit positions within the patches, the corresponding patch number of the dispersed seed is calculated from the coordinates (x_{seed}, y_{seed}).

The sum of those produced seeds, which are dispersed to a certain patch are added first to its corresponding seed pool N_{pool} before they are able to germinate and establish in the next time step.

D.3 Germination of seeds

Before seeds can germinate from the seed pool and establish successfully, light and space conditions are checked. Per type a minimum number of seeds can be withheld in the seed

pool, which is by default set to 0.

For determining the light conditions, the incoming irradiance on the floor is divided by the incoming irradiance above canopy (see Appendix F for their calculation). This results in the percentage of incoming irradiance on the floor I_{floor}, which is possibly reduced due to shading of already existing individuals. Dependent on a minimum percentage of light I_{seed} required for seed germination and seedling establishment for each type, it is checked whether I_{floor} is sufficient:

$$N_{germ} = \begin{cases} N_{pool} & ,I_{floor} \geq I_{seed} \\ 0 & ,I_{floor} < I_{seed} \end{cases}, \tag{13}$$

whereby N_{germ} is the number of germinated seedlings.

If light requirements are not sufficient for seeds of a specific type, they remain in the seed pool and may germinate in future time step as far as conditions become favorable. By this, seeds may accumulate in the seed pool if light conditions remain unfavorable over a period of time.

Seeds waiting in the seed pool for favorable germination conditions may be affected by seed pool mortality. For each type a mortality rate M_{pool} [$^1/_{\mathrm{yr}}$] is defined prior to the start of the simulation. A rate of $M_{pool} = 0$ represents, for example, an unlimited accumulation of seeds in times of unfavorable conditions. In contrast, a rate of $M_{pool} = 1$ would not allow any accumulation of seeds in the seed pool.

The density of germinated seedlings can be additionally regulated. Thereby, for each type and patch the number N_{germ} is truncated at a predefined value max_{dens}.

D.4 Establishment of seedlings

If light requirements are fulfilled for successful seedling germination, it is secondly checked whether enough space is available for their establishment. Germinated seedlings start with a predetermined stem diameter D_{min}, irrespective of type or species. Using the chosen functional relationships describing the geometry of an individual (see Appendix C), their corresponding height H_{min} can be calculated. If space at the respective height is already filled by more than 100% with existing individuals, none of the germinated seedlings would be able to establish:

$$N_{est} = \begin{cases} N_{germ} & ,CCA_l < 1 \\ 0 & ,CCA_l \geq 1 \end{cases}, \tag{14}$$

whereby N_{est} is the number of successfully established seedlings and CCA_l denotes the cumulative crown area at the height layer l (of width Δh [m]) which correspond to H_{min}:

$$l = \left\lfloor \frac{H_{min}}{\Delta h} \right\rfloor . \tag{15}$$

see Appendix E for the calculation of the cumulative crown area CCA of all height layer of the aboveground discretized space.

Appendix E Mortality

In FORMIND 3.0 trees can die due to various reasons. The following different types of mortality occur in a serial way:

- background mortality M_B
- mortality dependent on an individual's stem diameter M_D
- mortality dependent on an individual's diameter increment M_I
- crowding mortality due to limited space
- mortality due to damage by a falling tree
- mortality due to fragmentation

Individual trees of the same type and size, which are located in the same patch, are summarized in this section by a so-called **cohort**. Each cohort is uniquely described by its type, the number of identical trees (N), their age and the size of one single tree (i.e. aboveground biomass). In this section, the number of identical trees in a cohort change due to mortality processes. In the following, we describe the different types of mortality in more detail.

E.1 General mortality

In contrast to the later described event-driven forms of mortality, there is a general mortality rate per tree which is active in each time step t_y. This mortality rate M is calculated as the sum of the background mortality rate M_B and two further mortality rates dependent on the stem diameter M_D as well as its increment M_I:

$$M = M_B + M_D + M_I. \tag{16}$$

The background mortality M_B [$^1/_{\mathrm{yr}}$] is a type-specific constant input parameter.

The mortality rate M_D depends on the stem diameter D [m] and provides the possibility to give older trees (with a bigger stem diameter) a higher mortality rate than younger trees or vice versa. The rate is calculated by:

$$M_D(D) = m_{d0} \cdot D^{m_{d1}}, \tag{17}$$

whereby m_{d0} and m_{d1} are type-specific parameters.

The mortality rate M_I depends on the increment of the stem diameter D [mm] per time step t_y and provides the possibility to include a higher mortality for older trees or those under stress. It is modelled by the functional relationship:

$$M_I(\Delta D) = m_{i0} + m_{i1}\ \Delta D + m_{i2}\Delta D^2, \tag{18}$$

where m_{i0}, m_{i1} and m_{i2} are type-specific parameters. The increment of the stem diameter from time t to time $t + t_y$ is denoted as ΔD.

The trees per patch die according to their mortality rate M - either stochastically or deterministically.

Deterministic dying is active if the number of individuals per cohort is greater than a predefined number N_M **and** if the stem diameter of each individual is smaller than a predefined threshold D_M. In this case, the number of dying trees per cohort is determined by:

$$N_Y = N \cdot M, \tag{19}$$

where N is the number of trees per cohort, N_Y is the number of dying trees per cohort and M is the calculated mortality rate per time step t_y. The number of dying trees N_Y is rounded by $\lfloor N_Y + 0.5 \rfloor$.

In the contrary case (i.e. $N < N_M$ **or** $D > D_M$), deaths occur stochastically. That means, for each tree the mortality rate M represents its probability of dying (i.e. by comparing a random number from a uniform distribution in the range of [0;1] with the mortality rate M):

$$N_Y = \sum_{j=1}^{N} \delta_{rM}, \tag{20}$$

where N is the number of trees per cohort, N_Y is the number of dying trees per cohort, M is the calculated mortality rate per time step t_y and r is a random number from a uniform distribution in the range of [0;1]. The symbol δ_{rM} is defined as:

$$\delta_{rM} = \begin{cases} 1 & , r \leq M \\ 0 & , r > M \end{cases} \tag{21}$$

E.2 Crowding mortality

Crowding occurs, if at any height layer the cumulative crown area of all trees on a patch exceeds A_{patch}. At first, the cumulative crown area CCA [m^2/m^2] of all trees on a patch is calculated for each height layer i relative to the patch area A_{patch}:

$$CCA_i = \frac{1}{A_{patch}} \cdot \sum_{\substack{all\ individuals \\ with\ l_{min} \le i \le l_{max}}} C_A, \tag{22}$$

where C_A is the crown projection area of a tree (see Appendix C). Thereby, each tree occupies only a limited amount of height layers (i.e. between layer l_{min} and l_{max}) defined by the individual's crown length C_L [m] and its height H [m]:

$$l_{max} = \left\lfloor \frac{H}{\Delta h} \right\rfloor \tag{23}$$

$$l_{min} = \left\lfloor \frac{H - C_L}{\Delta h} \right\rfloor \tag{24}$$

Mortality due to crowding is calculated per tree represented by a reduction factor R_c [-]. This individual reduction factor is calculated based on those height layers, which the individual's crown is occupying (Fig. 4).

The reduction factor R_c is determined by the reciprocal of the maximum cumulative crown area according to those height layers between the individual limits l_{min} and l_{max}:

$$R_c = \frac{1}{\max\limits_{i \in [l_{min}; l_{max}]} (CCA_i)}. \tag{25}$$

If the maximum cumulative crown area of any height layer, which the individual's crown is occupying, exceeds A_{patch} (i.e. $CCA_i > 1$), the individual reduction factor R_c falls below the threshold of 0.99. In this case, the number of dying identical trees per cohort N_C is calculated by:

$$N_C = N\ (1 - R_c). \tag{26}$$

Mortality due to crowding (or self-thinning) can be interpreted as competition for space. Besides crowding, the vertical discretization of the aboveground space is also important for the light climate calculations. To save computation time, the calculation of R_c is coupled to that of the light climate which is explained in Appendix F.

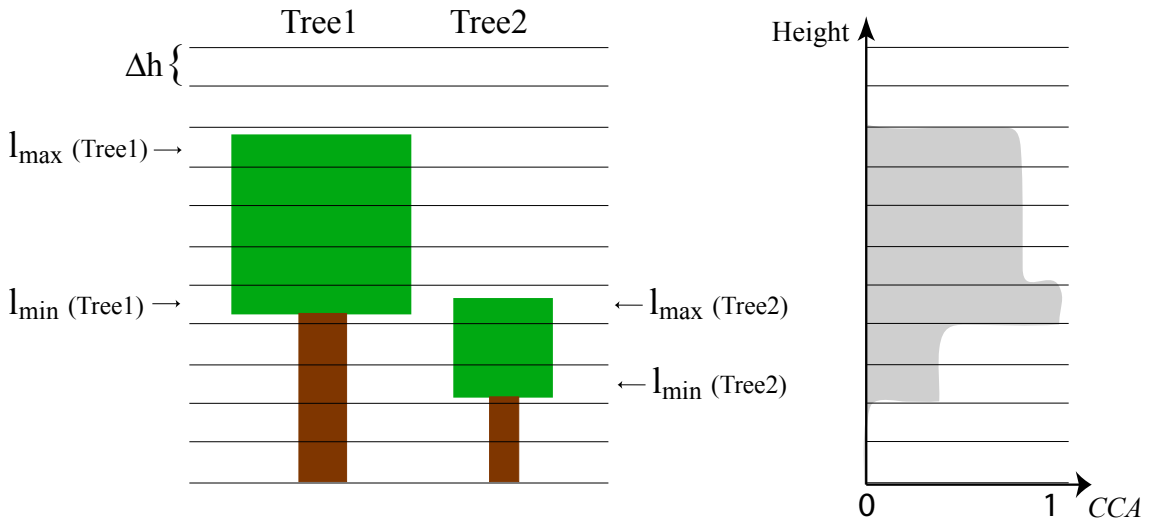

Figure 4: *Illustration of crowding on the example of two single trees . The limits of each crown are shown by $l_{min}(Tree1)$, $l_{max}(Tree1)$, $l_{min}(Tree2)$ and $l_{max}(Tree2)$. The vertically discretized aboveground space into height layers of width Δh [m] is coloured differently according to the sum of the crown projection areas of both individuals occupying the layers. The darker the colour is, the more crowns occupy the respective height layer. This is calculated by the cumulative crown area CCA [-] relative to the patch area, which is illustrated on the right side. The maximum of CCA is used to calculate the reduction factor R_c for each individual. In this example, the reduction factor for each of both trees is calculated based on the 5. height layer from the bottom (equal to layer $l_{min}(Tree1)$ and $l_{max}(Tree2)$).*

E.3 Tree fall mortality

If a tree falls, neighboring trees can be destroyed. A dying tree falls down with probability f_{fall}. The falling target patch depends on falling direction and on tree height H. Falling direction DIR (drawn from a uniform distribution in the range of [0°, 360°]) is chosen randomly. The target coordinates of the falling tree (x_{fall}, y_{fall}) are determined in the following way:

$$x_{fall} = x_{tree} + H \ sin\left(2 \ \pi \ \frac{DIR}{360}\right) \tag{27}$$

$$y_{fall} = y_{tree} + H \ cos\left(2 \ \pi \ \frac{DIR}{360}\right) \tag{28}$$

whereby (x_{tree}, y_{tree}) is the standing position of the falling tree . With this target coordinates the affected patch is determined. All smaller trees (tree height $< H$) in this target patch are dying with a damage rate M_{dam}:

$$M_{dam} = C_A / A_{patch}, \tag{29}$$

whereby C_A is the crown area of the falling tree and A_{patch} the area of the target patch.

The trees in the target patch die according to the damage rate M_{dam} - either stochastically or deterministically. Deterministic dying is active if the number of trees per cohort is greater than 100. In this case, the number of dying trees per cohort N_F is determined by multiplying number of trees N per cohort with damage rate M_{dam}.

$$N_F = N \cdot M_{dam}, \tag{30}$$

The number of dying trees N_F is rounded by $\lfloor N_F + 0.5 \rfloor$.

In the contrary case (less than 100 trees per cohort), stochastic dying is performed. That means, for each tree the damage rate M_{dam} represents its probability of dying (i.e. by comparing a random number from a uniform distribution in the range of $[0; 1]$ with the damage rate).

$$N_F = \sum_{j=1}^{N} \delta_{rM_{dam}}, \tag{31}$$

where N is the number of trees per cohort, N_F is the number of dying trees per cohort, M_{dam} is the damage rate per time step t_y and r is a random number from a uniform distribution in the range of $[0; 1]$. The symbol $\delta_{rM_{dam}}$ is defined as:

$$\delta_{rM_{dam}} = \begin{cases} 1 & , r \leq M_{dam} \\ 0 & , r > M_{dam} \end{cases} \tag{32}$$

E.4 Change of mortality due to fragmentation

It has been observed that mortality is increased and tree species richness is reduced at forest edges, and that large trees are often missing in small fragments (Ferreira and Laurance, 1997; Laurance et al., 1998b, Arroyo-Rodriguez and Mandujano, 2006; Laurance et al., 2000, Pimentel Lopes de Melo et al. 2006). The extent of forest edges varies between forest regions. For example, increased edge mortality could be measured up to 100 m into the forest interior in the Amazon (Ferreira and Laurance, 1997).

In FORMIND 3.0 we model increased mortality at the edge of forest fragments by multiplying the general mortality M with a fragmentation variable m_{frag}. Thus, the additional mortality due to fragmentation can be calculated as:

$$M_{frag} = M \cdot (m_{frag} - 1). \tag{33}$$

We assume that the fragmentation induced mortality M_{frag} is higher at forest edges ($<$ 100 m) than in the interior. Thus, the value of m_{frag} is modelled dependent on the distance to the fragment edges (Tab. 3). In addition, large trees ($D > 60$ cm) can suffer an increased mortality.

Table 3: *Mortality increase due to fragmentation, dependent on the distance to a fragment edge and on the stem diameter D [cm] of a tree .*

Distance to edge	Value of m_{frag} ($D \leq 60$)	Value of m_{frag} ($D > 60$)
0 - 20 m	2.5	4
20 - 40 m	1.75	2.5
40 - 60 m	1.375	1.75
60 - 80 m	1.1875	1.375
80 - 100 m	1.09375	1.1875

If this type of mortality is activated, we recommend to choose a patch size of 20 m x 20 m (i.e. $A_{patch} = 400$ m^2) according to the distance classes in Table 3.

The number of additional trees that die due to fragmentation effects can be calculated as:

$$N_{frag} = N \cdot M_{frag}. \tag{34}$$

E.5 Overall change in number of trees per cohort

Overall, per time step Δt and for each cohort the change in the number of trees per cohort N is determined by:

$$dN/dt = -(N_Y + N_C + N_F + N_{frag}), \tag{35}$$

where N_Y is the number of trees dying due to regular mortality, N_C is the number of trees dying due to crowding, N_F is the number of trees dying due to damages caused by a falling tree and N_{frag} is the number of trees dying due to increased mortality near fragment edges.

The amount of above ground carbon S_{mort} [$^{t_C}/_{\text{ha}}$], which results from the death of trees within the current time step is calculated by:

$$S_{mort} = 0.44 \cdot \sum_{all\ cohorts} (N_Y + N_C + N_F + N_{frag}) \cdot B, \tag{36}$$

where B is the above ground biomass of the tree (see Appendix C). We assume that 1 g organic dry matter contains 44 % carbon [Larcher, 2001].

Appendix F Competition and environmental limitations

F.1 Light climate

A single tree on a patch receives full incoming radiation. An increasing number of individual trees of differing heights on a patch results in shading within the canopy. Higher trees intercept radiation, which is not available for smaller individuals. Thus, with decreasing height from the canopy down to the ground, radiation is decreasing. We call this vertical distribution of light availability within a patch 'light climate'.

To calculate the light availability in different heights within the canopy, the vertical discretization of the above-ground space is used (i.e. height layers of constant width Δh). For each patch and height layer, the leaf area accumulated by all trees on the patch is calculated. Each tree contributes parts of its crown leaf area to those height layers, which are occupied by its crown (i.e. height layers from l_{min} to l_{max}). These limits are determined by the individual's crown length C_L and its height H:

$$l_{max} = \left\lfloor \frac{H}{\Delta h} \right\rfloor \tag{37}$$

$$l_{min} = \left\lfloor \frac{H - C_L}{\Delta h} \right\rfloor. \tag{38}$$

The number of height layers a tree is occupying by its crown (n_{layer}) can then be calculated by:

$$n_{layer} = l_{max} - l_{min}. \tag{39}$$

For those height layers between l_{min} and l_{max}, an individual's leaf area contributes equally to each layer i:

$$\bar{L}_i = \frac{LAI \cdot C_A}{n_{layer}}, \tag{40}$$

whereby $\bar{L}_i$ [m^2] represents the contribution of an tree 's leaf area to the layer i, LAI [-] is the leaf area index of the tree (see C.6) and C_A [m^2] is crown projection area of the tree 's crown. The multiplication of LAI by C_A results in the leaf area in [m^2] of an single tree . Summing up all contributions of the trees ' leaf area per patch to their respective occupied height layers and relative to the patch area, results in the patch-based leaf area index $\hat{L}_i$ [-] per layer i:

$$\hat{L}_i = \frac{1}{A_{patch}} \sum_{\substack{all\ individuals \\ with\ l_{min} \le i \le l_{max}}} \bar{L}_i, \tag{41}$$

where $\bar{L}_i$ [m^2] represents the leaf area contribution of an tree to the height layer i and A_{patch} [m^2] denotes the area of a patch.

Using this information, the radiation each tree is able to intercept can be determined. Light attenuation through the canopy is calculated using the approach of [Monsi and Saeki, 1953]. The incoming radiation I_{ind} on top of a tree (i.e. on top of the height layer l_{max} the tree is reaching) is calculated by:

$$I_{ind} = I_0 \cdot exp\left(-k \cdot \sum_{i>l_{max}} \hat{L}_i\right), \tag{42}$$

where the sum in the exponent accumulates the patch-based leaf area indices of all height layers above the individual's height. The parameter k denotes the light extinction coefficient [-] of a tree , I_0 [μmol (photons)/m^2 s] is the daily radiation above canopy averaged from sunrise to sunset during the vegetation period and $\hat{L}_i$ [-] represents the patch-based leaf area index of height layer i.

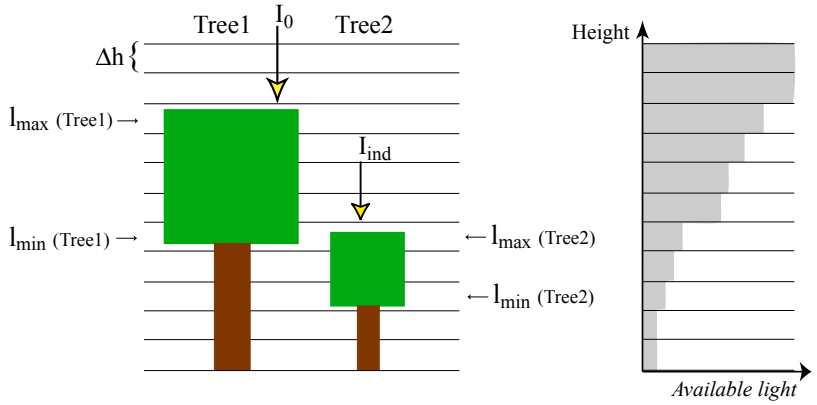

Figure 5: *Illustration of the light climate on the example of two single trees . The limits of each crown are shown by l_{min} (Tree1), l_{max}(Tree1), l_{min}(Tree2) and l_{max}(Tree2). The vertically discretized aboveground space into height layers of width Δh [m] is coloured differently according to the available radiation. The lighter the colour is, the more attenuated the radiation is, which results from the absorption by higher individuals' leaves. On the right hand side the decrease of available light from the canopy to the floor is illustrated by the grey polygon. Thereby, attenuation is greatest in the height layer both trees occupy by their crowns (i.e. layer l_{min}(Tree1) and l_{max}(Tree2)).*

By determining the available radiation for each single tree (at the top of the crown), competition for light between trees is considered.

F.2 Water cycle and soil water limitation

Individual trees take up soil water resources to fulfill the requirements for their gross productivity. We determine an individual's uptake of soil water based on its demand and on the total available soil water.

Firstly, the soil water content Θ_{soil} is computed preliminary on an hourly basis using a differential equation, which quantifies preliminary hourly changes in the soil water content per patch depending on precipitation PR, interception IN and run-off RO (Fig. 6, cf. [Kumagai et al., 2004]):

$$\frac{d\Theta_{soil}}{dt} = PR(t) - IN(t) - RO(t). \tag{43}$$

The resulting soil water content represents the total available soil water before soil water uptake by individuals. Uptake of soil water resources by trees is modelled equal to their transpiration and subtracted from Θ_{soil} later within the timestep (see eqn. 54).

The **interception** IN [mm/h] is calculated dependent on the total leaf area index per patch (i.e. $\sum_i \hat{L}_i$ in [-], cf. [Liang et al., 1994]):

$$IN(t) = min(K_L \cdot \left(\sum_i \hat{L}_i\right), PR(t)), \tag{44}$$

where K_L [mm/h] is the interception constant and PR [mm/h] denotes the precipitation.

On the ground surface of a patch, we consider two different run-offs: surface run-off and subsurface run-off:

$$RO(t) = RO_{\rightarrow}(t) + RO_{\downarrow}(t), \tag{45}$$

where **surface run-off** $RO_{\rightarrow}$ [mm/h] is defined in the following way:

$$RO_{\rightarrow} = max(0, \Theta_{soil}(t) + PR(t) - IN(t) - POR) \tag{46}$$

with POR [mm/h] denoting the soil porosity (i.e. defined as the maximum water intake of the soil per patch).All additional incoming water is assumed to be surface run-off.

For the calculation of the **subsurface run-off** $RO_{\downarrow}$ due to gravitation, we use the Brooks-Corey relation (cf. [Liang et al., 1994]):

$$RO_{\downarrow} = K_s \cdot \left(\frac{\Theta_{soil}(t) - \Theta_{res}}{POR - \Theta_{res}}\right)^{\frac{2}{\lambda}+3}, \tag{47}$$

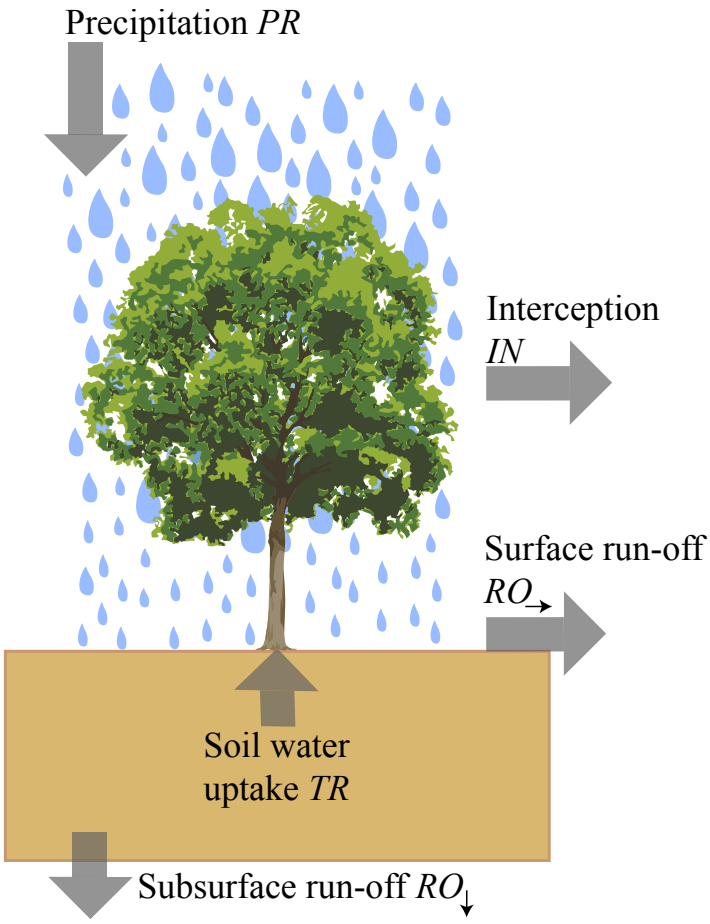

Figure 6: *Illustration of the water cycle on the example of a single tree .*

where K_s [mm/h] is the fully saturated conductivity, Θ_{res} [mm/h] the residual water content, and λ [-] the pore size distribution index.

The preliminary soil water content Θ_{soil} represents the soil water content, which is available for the individuals' uptake or transpiration. To calculate the **transpiration** TR [mm/h] of all trees per patch, we use the water-use-efficiency concept (cf. [Lambers et al., 2008]):

$$TR = \frac{1}{A_{patch}} \sum_{all\ trees} \frac{GPP}{WUE}, \tag{48}$$

whereby GPP in $[g_{ODM}/\text{h}]$ denotes the hourly gross primary production of an individual on the patch (see Appendix G). Please note, that we simulate GPP per time step t_y. To calculate GPP on an hourly basis, we divide GPP $[g_{ODM}/\Delta t]$ by the number of hours within the time step Δt. The constant type-specific value WUE in $[g_{ODM}/kg_{H_2O}]$ represents the water-use-efficiency parameter and A_{patch} [m^2] the area of a patch.

The resulting transpiration TR may be limited in three ways calculated in a serial way:

PET limitation Transpiration can be limited by the potential evapotranspiration PET [mm/h] and the interception IN [mm/h] (calculated by eqn. 44):

$$TR_{new} = \begin{cases} TR(t) & , TR(t) \leq PET(t) - IN(t) \\ PET(t) - IN(t) & , TR(t) > PET(t) - IN(t) \end{cases}. \tag{49}$$

Soil water limitation Transpiration can be limited by the preliminary soil water content Θ_{soil} [mm/h] (calculated by eqn. 43) and the permanent wilting point Θ_{pwp} [mm/h]:

$$TR_{new}(\Theta_{soil}) = \begin{cases} TR(t) & ,\Theta_{soil}(t) - TR(t) \geq \Theta_{pwp} \\ \Theta_{soil}(t) - \Theta_{pwp} & ,\Theta_{soil}(t) - TR(t) < \Theta_{pwp} \\ 0 & ,\Theta_{soil}(t) \leq \Theta_{pwp} \end{cases}. \tag{50}$$

Competition for water Competition between trees can limit the transpiration in the following way:

$$TR = \varphi_W(\Theta_{soil}) \cdot TR(t), \tag{51}$$

where φ_W [-] represents a reduction factor ranging between 0 and 1, depending on the actual soil water content.

The reduction factor φ_W is calculated using the approach of [Granier et al., 1999], which is based on the preliminary soil water content (calculated by eqn. 43):

$$\varphi_W(\Theta_{soil}) = \begin{cases} 0 & ,\Theta_{soil}(t) \leq \Theta_{pwp} \\ \frac{\Theta_{soil}(t)-\Theta_{pwp}}{\Theta_{msw}-\Theta_{pwp}} & ,\Theta_{pwp} < \Theta_{soil}(t) < \Theta_{msw} \\ 1 & ,\Theta_{soil}(t) \leq \Theta_{msw} \end{cases}, \tag{52}$$

where Θ_{pwp} is the permanent wilting point in $[V\%]$ and Θ_{msw} is the minimum soil water content in $[V\%]$. For the purpose of the calculation of eqn. 52 only, Θ_{soil} needs to be converted from [mm/h] to [V%]. Thereby, the soil is modelled down to a constant depth [m] defined prior to the start of the simulation.

The minimum soil water content (Θ_{msw}) is determined according to [Granier et al., 1999] by:

$$\Theta_{msw} = \Theta_{pwp} + 0.4(\Theta_{fc} - \Theta_{pwp}) \tag{53}$$

whereby Θ_{fc} denotes the field capacity in $[V\%]$.

The soil water content in the next day step is then calculated by the difference between the preliminary soil water content (calculated by eqn. 43) and the (eventually limited) transpiration TR:

$$\frac{d\Theta_{soil}}{dt} = \Theta_{soil}(t) – TR(t). \tag{54}$$

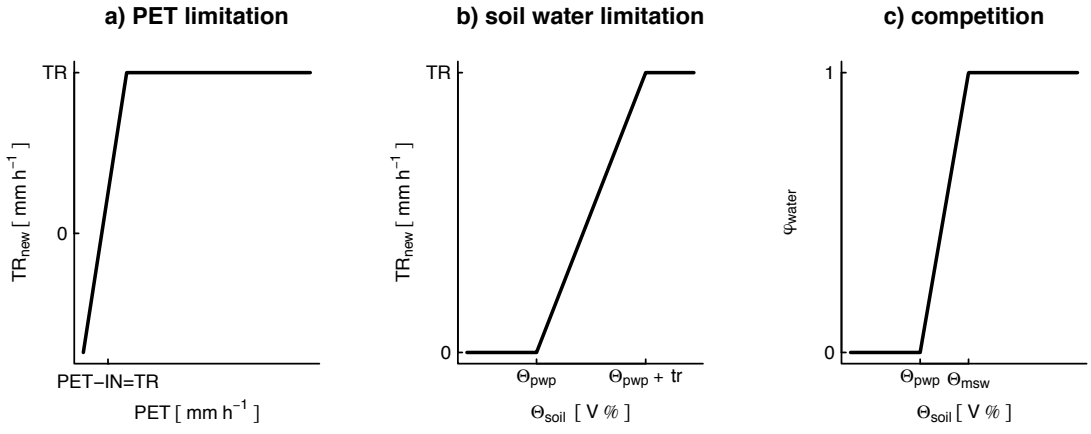

Figure 7: *Water limitation function. a) limitation of TR due to PET. b) limitation of TR due to Soil water. c) φ_{water} as function of Soil water.*

F.3 Temperature

The gross primary production GPP $[t_{ODM}/t_y]$ of a tree (see Appendix G) may be influenced by phenology (esp. in the temperate zone) and air temperature. Respiration for maintenance purposes of an individual (see Appendix G) may also be affected by air temperature. The influence on both - gross productivity and respiration, is modelled using limitation factor, by which they are simply multiplied (see Appendix G). In the following, we describe the calculations of these limitation factors:

Phenology

Individual trees make photosynthesis only during their photosynthetic active period. In the **temperate zone**, we distinguish between broad-leaf and needle-leaf trees . Only deciduous broad-leaf trees have two phenology phases: (i) a dormant phase during winter and (ii) a photosynthetic active period of φ_{act} [days] after bud-burst until fall (i.e. the vegetation period).

The date of bud-burst is reached, if the temperature sum (daily mean air temperatures $> 5°$) since 1 January is higher than a critical temperature T_{crit} [Sato et al., 2007]:

$$T_{crit} = -68 + 638\ e^{-0.01 \cdot n}, \tag{55}$$

where n is the number of days per time step Δt with an air temperature below 5° since 1 November of the previous year. This algorithm is based on the global distribution of leaf onset dates estimated from remote sensing data [Botta et al., 2000]. The photosynthetic active period stops if the 10-day moving average of daily mean air temperatures falls below $9°C$ [Sato et al., 2007].

In contrast to the broad-leaf trees, the photosynthetic active period φ_{act} of needle-leaf trees amounts a complete year of 365 days (without any dormant phase).

In the **tropical zone**, we assume for all individuals irrespective of their type a complete photosynthetic active period with $\varphi_{act} = 365$ days.

Temperature limitation of gross productivity

The gross primary production of a tree can be reduced due to air temperatures. A corresponding limitation factor φ_T is calculated by averaging the reduction factors over the whole time step Δt:

$$\varphi_T = \frac{1}{n} \sum_{1}^{n} \varphi_{T,l} \cdot \varphi_{T,h}, \tag{56}$$

where n is the number of days per time step Δt and the values $\varphi_{T,l}$ and $\varphi_{T,h}$ are the daily inhibition factors for low and high air temperatures [Gutiérrez and Huth, 2012; Haxeltine and Prentice, 1996].

The **reduction factor for low air temperatures** $\varphi_{T,l}$ $[°C]$ is calculated by:

$$\varphi_{T,l} = \left(1 + e^{k_0 \cdot k_1 - T}\right)^{-1}, \tag{57}$$

where T $[°C]$ is the daily mean air temperature and k_0 and k_1 are type-specific parameters.

These parameters k_0 and k_1 are calculated by:

$$k_0 = \frac{2\ ln(0.01/0.99)}{T_{CO_2,l} - T_{cold}} \tag{58}$$

$$k_1 = 0.5\ (T_{CO_2,l} + T_{cold}) \tag{59}$$

where $T_{CO_2,l}$ $[°C]$ and T_{cold} $[°C]$ are type-specific parameters representing the lowest temperature limit for CO_2 assimilation and the monthly mean air temperature of the coldest month an individual can cope with, respectively.

Similarly, the **inhibition factor for high air temperatures** $\varphi_{T,h}$ in $°C$ is calculated by:

$$\varphi_{T,h} = 1 - 0.01 \cdot e^{k_2\ (T - T_{hot})} \tag{60}$$

where k_2 is a type-specific parameter, T $[°C]$ is the daily mean temperature and T_{hot} $[°C]$ is the type-specific mean temperature of the hottest month an individual can occur.

The parameter k_2 is calculated as:

$$k_2 = \frac{ln(0.99/0.01)}{T_{CO_2,h} - T_{hot}}, \tag{61}$$

whereby $T_{CO_2,h}$ $[°C]$ and T_{hot} $[°C]$ are type-specific parameters representing the higher temperature limit for CO_2 assimilation and the monthly mean air temperature of the warmest month an individual can cope with, respectively.

Temperature limitation of maintenance respiration

Maintenance respiration is assumed to change exponentially with air temperature represented by the limitation factor κ_T [Prentice et al., 1993]:

$$\kappa_T = \frac{1}{n} \sum_{1}^{n} Q_{10}^{\left(\frac{T - T_{ref}}{10}\right)}, \tag{62}$$

where n is the number of days per time step t_y, T [$^\circ C$] is the daily mean air temperature, Q_{10} [-] and T_{ref} [$^\circ C$] are constant parameters, irrespective of type. T_{ref} represents the reference temperature, at which maintenance respiration is not influenced. Air temperatures below T_{ref} result in a decrease of maintenance respiration ($\kappa_T < 1$) and those above T_{ref} in an increase of maintenance respiration ($\kappa_T > 1$).

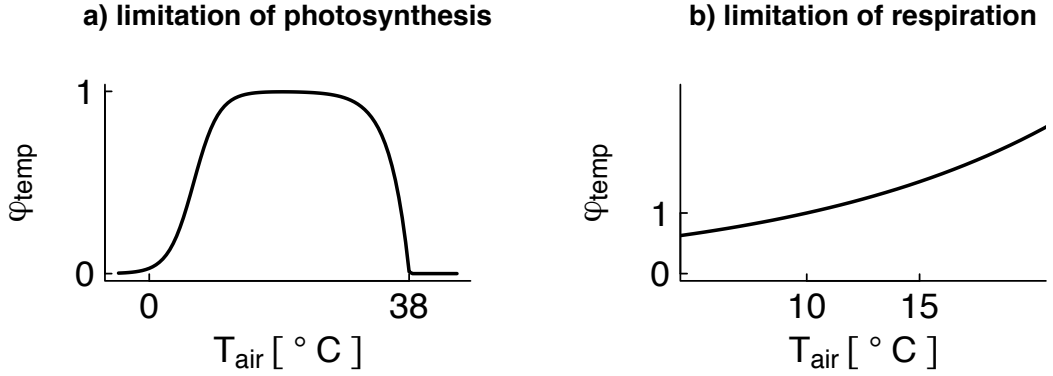

Figure 8: *Temperature limitation function. a) limitation factor of Photosynthesis. b) limitation factor of maintenance respiration.*

Appendix G Growth of a tree

G.1 Interim photosynthesis

Based on the incoming irradiance on top of a tree I_{ind} (see Appendix F), organic dry matter is produced via gross photosynthesis. In this section the interim photosynthesis is calculated without reduction due to limited soil water availability nor temperature effects.

The interim gross photosynthesis P_{ind} of an individual is modelled using the approach of [Thornley and Johnson, 1990]. It is based on the single-leaf photosynthesis modelled by a Michaelis-Menten function – a typical saturation function describing the relation between the radiation I_{leaf} available on top of a leaf and its gross photosynthetic rate P_{leaf}:

$$P_{leaf}(I_{leaf}) = \frac{\alpha \cdot I_{leaf} \cdot p_{max}}{\alpha \cdot I_{leaf} + p_{max}}, \tag{63}$$

where α is the quantum efficiency, also known as the initial slope of the type-specific light response curve, I_{leaf} is the incoming irradiance on top of the surface of a single leaf within the individual's crown and p_{max} is the maximum leaf gross photosynthetic rate.

To obtain the incoming irradiance on top of the surface of a single leaf I_{leaf}, the available irradiance I_{ind} on top of the entire individual has to be modified:

$$I_{leaf}(L) = \frac{k}{1-m}\ I_{ind} \cdot e^{-k \cdot L}, \tag{64}$$

where k [-] is the type-specific light extinction coefficient, m [-] represents the transmission coefficient and I_{ind} denotes the available incoming irradiance on top of a tree .

The first part $\frac{k}{1-m}\ I_{ind}$ in eqn. (64) is correcting the incoming irradiance in order to obtain those parts, which can be absorbed by a leaf. The second part $e^{-k \cdot L}$ in eqn. (64) accounts for self-shading within the individual's crown. As the leaves of an individual are assumed to be homogeneously distributed within its crown, some leaves will be shaded by higher ones within the crown. Thereby, $L = 0$ represents the top of the individual and $L = LAI$ represents the bottom of the individual's crown with LAI being its leaf area index (see Appendix C).

To obtain the interim gross photosynthetic rate of a tree per year P_{ind}, the single-leaf photosynthesis of eqn. (63) is integrated over the individual's leaf area index LAI (see Appendix C):

$$P_{ind} = \int_0^{LAI} P_{leaf}(I_{leaf}(L))dL. \tag{65}$$

The integration results in the interim photosynthesis of an tree per year [Thornley and Johnson, 1990]:

$$P_{ind} = \frac{p_{max}}{k} \cdot ln \frac{\alpha \; k \; I_{ind} + p_{max}(1-m)}{\alpha \; k \; I_{ind} \; e^{-k \cdot LAI} + p_{max}(1-m)}. \tag{66}$$

To convert the interim photosynthesis P_{ind} from $[\mu mol_{CO_2}/m^2 s]$ to $[t_{ODM}/y]$, P_{ind} has to be multiplied by the individual's crown area C_A (see Appendix C), the type-specific photosynthetic active period φ_{act} and finally a conversion factor c_{odm}:

$$P_{ind} \cdot C_A \cdot 60 \cdot 60 \cdot l_{day} \cdot \varphi_{act} \cdot \varphi_{odm}, \tag{67}$$

where the multiplication by $60 \cdot 60$ accounts for the conversion from seconds to hours. The factor l_{day} [h] represents the mean day length during the vegetation period φ_{act} [d] (see Appendix F). The conversion factor $\varphi_{odm} = 0.63 \cdot 44 \cdot 10^{-12}$ includes the molar mass of CO_2, the conversion from g to t and the conversion from CO_2 to organic dry mass ODM [Larcher, 2001].

G.2 Gross primary production

The gross primary production GPP of a tree is calculated from the interim photosynthesis P_{ind} $[t_{ODM}/y]$ (see G.1):

$$GPP = P_{ind} \; \varphi_T \; \varphi_W, \tag{68}$$

where φ_W denotes the reduction factor accounting for limited soil water and φ_T represents the limitation factor of air temperature effect. Both factors range between 0 and 1 and thus, only reducing GPP in times of unfavorable conditions (see Appendix F).

G.3 Biomass increment of a tree

Gross primary production GPP of eqn. (68) is first used for the maintenance of the already existing aboveground biomass of an tree . Costs for maintenance are modelled as biomass losses in terms of maintenance respiration R_m $[t_{ODM}/y]$. The remaining productivity $(GPP - R_m)$ is then available for growth of new aboveground biomass. Costs for the production of new structural tissue are modelled also as biomass losses in terms of growth respiration. This results in the net productivity ΔB [Dislich et al., 2009]:

$$\Delta B = (1 - r_g) \; (GPP - R_m), \tag{69}$$

where r_g [-] represents a constant parameter describing the fraction of $(GPP - R_m)$ attributed to growth respiration. In contrast, maintenance respiration R_m is modelled proportionally to the already existing aboveground biomass of a tree (see G.4).

G.4 Maintenance respiration

The maintenance respiration R_m of a tree is calculated inversely by rearranging eqn. (69):

$$R_m = GPP - \frac{\Delta B}{1 - r_g}. \tag{70}$$

Maintenance respiration R_m is further modelled proportional to the already existing aboveground biomass B $[t_{ODM}]$ of an individual:

$$R_m = \kappa_T \cdot r_m \cdot B, \tag{71}$$

where r_m denotes the maintenance respiration rate $[1/y]$ and κ_T represents a limitation factor dependent on air temperature (see Appendix F).

Combining equation (70) with equation (71) and arranging in terms of the respiration rate r_m results in:

$$r_m = \frac{1}{B \cdot \kappa_T} \cdot \left(GPP - \frac{\Delta B}{1 - R_g} \right). \tag{72}$$

In FORMIND 3.0 we have two different approaches of calculating the maintenance respiration rate based on eqn. (72):

- Optimal approach (no limitation)
- Observation-based approach

In the following, we describe both approaches in more detail.

Optimal approach (most frequently used)

The maintenance respiration rate r_m of eqn. (72) is calculated using the assumption of full resource availability. Thereby, it is assumed that full resource availability (i.e. no limitation by shading, soil water or air temperature) results in the observed maxima of field measurements of stem diameter increments:

$$r_m = \frac{1}{B} \cdot \left(P_{ind}(I_0) - \frac{B(D + g(D)) - B}{(1 - R_g)} \right), \tag{73}$$

where this equation can be obtained by substituting in eqn. (72) (i) κ_T by 1, (ii) GPP by the gross productivity under full resource availability $P_{ind}(I_0)$ (see eqn. 67) with I_0 as the full available incoming irradiance and (iii) ΔB by the biomass increment derived from the maximum stem diameter increment under full resource availability $D + g(D)$ using the individual's geometry (see Appendix C). See G.5 for different modelling approaches of the *maximum diameter growth curve* $g(D)$.

This approach is proposed when climate data at the time of field measurements are not available.

Observation-based approach

In this approach, the maintenance respiration rate r_m is calculated including those climatic conditions, which were observed during the field measurements of stem diameter increments. The correspondence of environmental factors (see Appendix F) to these climatic conditions during the observations is indicated by $\check{()}$.

$$r_m = \frac{1}{B} \cdot \left(GPP(\check{I_{ind}}, \check{\varphi_{act}}, \check{\varphi_T}, \check{\varphi_W}) - \frac{B(D + g(D)) - B}{(1 - R_g)} \right), \tag{74}$$

where this equation can be obtained by substituting in eqn. (72) (i) κ_T by 1, (ii) GPP by the gross productivity under the climate during observations $GPP(\check{I_{ind}}, \check{\varphi_{act}}, \check{\varphi_T}, \check{\varphi_W})$ and (iii) ΔB by the biomass increment derived from the maximum stem diameter increment using the individual's geometry $D + g(D)$ (see Appendix C). see G.5 for different modelling approaches of the *maximum diameter growth curve* $g(D)$.

This approach is proposed when climate data are available at the time field data on stem diameter increments were measured. In general, diameter increments are determined based on the difference of stem diameter measurements between two dates. For this time period climate data would be needed on which the limitation factors $\check{I_{ind}}$, $\check{\varphi_{act}}$, $\check{\varphi_T}$ and $\check{\varphi_W}$ of eqn. (74) can be calculated as described in Appendix F.

G.5 Maximum diameter growth curve

In the field, diameter increments can be determined by calculating the differences between two measurements of the stem diameter per tree (at two distinct observation dates). The increments are then usually plotted with the measured stem diameter of the first observation date to get an impression of how much a tree of stem diameter D is able to increase (see Fig. 9 for an example).

Such point clouds as illustrated in Fig. 9 can be described by functional relationships. Please note, that you have to adjust the increments according to a time step of 1 year. That means, if there is a period of e.g. 5 years between both observation dates of stem diameter measurements, you would have to correct the increments with respect to the smaller time scale.

Only a few information of the measured diameter increment curve are needed to derive:

- maximum diameter increment ΔD_{max} [m/y]
- stem diameter $D_{\Delta D_{max}}$ [% of D_{max}], which reaches ΔD_{max}

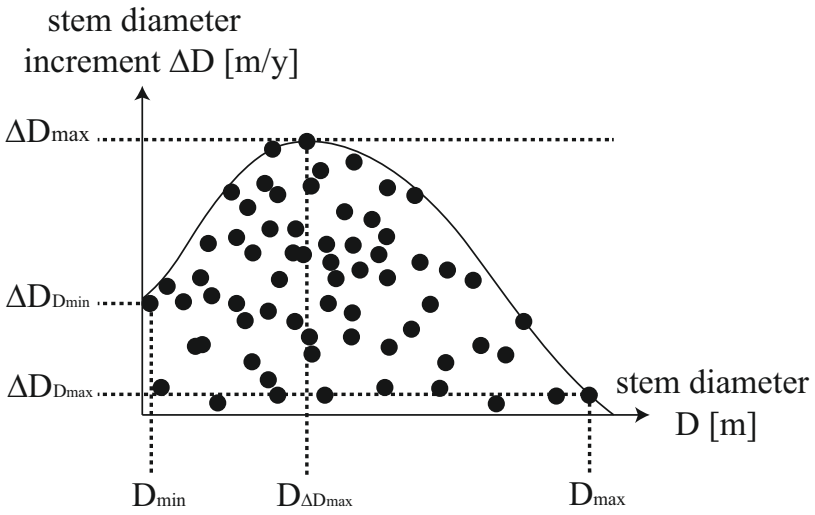

Figure 9: *Illustration of a measured diameter growth curve. Points represent illustrative measurements. The solid line represents a fitted growth function to the maximum values of the measurements. Dotted lines show important characteristics which would be needed for the first approach.*

- maximum diameter increment $\Delta D_{D_{min}}$ [% of ΔD_{max}] of the smallest possible tree (with $D = D_{min}$)
- maximum diameter increment $\Delta D_{D_{max}}$ [% of ΔD_{max}] of the biggest possible tree (with $D = D_{max}$)

Based on these characteristics, the coefficients of the growth function $g(D)$ can be calculated explicitly. In this model description, the Chanter approach is chosen as maximum growth curve. FORMIND offers also other growth curve approaches. If you are interested in the optional approaches, see www.formind.org.

Chanter approach

This approach describes the growth function $g(D)$ as follows:

$$g(D) = a_0 \cdot D \cdot \left(1 - \frac{D}{D_{max}}\right) \cdot e^{-a_1 \cdot D}, \tag{75}$$

where a_0 and a_1 are the type-specific coefficients, which are calculated by:

$$a_0 = \frac{e^{\frac{D_{max}-2\cdot(D_{\Delta D_{max}}\cdot D_{max})}{D_{max}-(D_{\Delta D_{max}}\cdot D_{max})}} \cdot D_{max} \cdot \Delta D_{max}}{(D_{max} - (D_{\Delta D_{max}} \cdot D_{max})) \cdot (D_{\Delta D_{max}} \cdot D_{max})}$$

$$a_1 = \frac{D_{max} - 2 \cdot (D_{\Delta D_{max}} \cdot D_{max})}{D_{max} \cdot (D_{\Delta D_{max}} \cdot D_{max}) - (D_{\Delta D_{max}} \cdot D_{max})^2},$$

whereby D_{max} is calculated out of maximum height (see C.7).
Please note, when determining the type-specific coefficients prior to the start of the simulation, that the curve represents growth under full resource availability. That means, not all measurements should be fitted, but only the maximum diameter increments (see Fischer, 2010 p. 55 for an example).

Table 4: *Summary of the morphological parameter range based on tropical parameterizations.*

parameter	values range	unit
ΔD_{max}	0.01 - 0.03	m
$D_{\Delta D_{max}}$	20 - 60	m
r_g	0.25	-

Appendix H Disturbance

Disturbances comprise the following scenarios:

- fire events, which affect trees depending on their fire resistance
- landslide events, which create bare soil

In total, N_D individuals of a cohort are dying due to disturbance induced mortality events.

H.1 Fire

Fire is the primary disturbance process affecting the terrestrial biosphere [Pfeiffer et al., 2013]. Especially wildfires affect species composition and vegetation structure in forests. They lead to a decrease of carbon storage and result in the emission of greenhouse gases. There is a long tradition in fire ecology to understand these processes and their interactions. Numerous methods were developed to estimate the disturbances due to fire events. Fire events are a complex distubances, which can be described by fire frequency, fire area and severity.

To understand the effect of fire on vegetation dynamics and vegetation structure, we developed the forest fire module ForFire, which is a combination of the ideas of well-established fire models [Gardner et al., 1999; Keane et al., 2004; Thonicke et al., 2001]. External inputs to the ForFire module are the mean fire frequency per hectare and year (λ in [years]), the mean fire size related to the investigated forest area (β in [%]) and the mean fire severity (s_{fire} [0-1]). Fire events are implemented on the patch level, i.e. the smallest possible fire size has the size of one patch (A_{patch}), the biggest fire considered are all patches of the simulation area.

- **fire events:** We implemented fire events in the following way: in every year a random number determines the number of fire events within this year. This fire frequency is poisson distributed [Green, 1989] with λ as mean time between fire events. If a fire event occurs, the fire centre is chosen randomly within the simulated forest area. The fire size (equal to the number of burned patches) is described by an exponential distribution β as mean size of the fire area related to the whole simulated forest area [Green, 1989]. The fire spread is modelled randomly: (i.) going from the fire centre every neighboring patch is burned, (ii.) a randomly burned patch is chosen and (iii.) again every neighboring patch is burned. This procedure is repeated until the number of the burned patches is equal to the specified fire size.

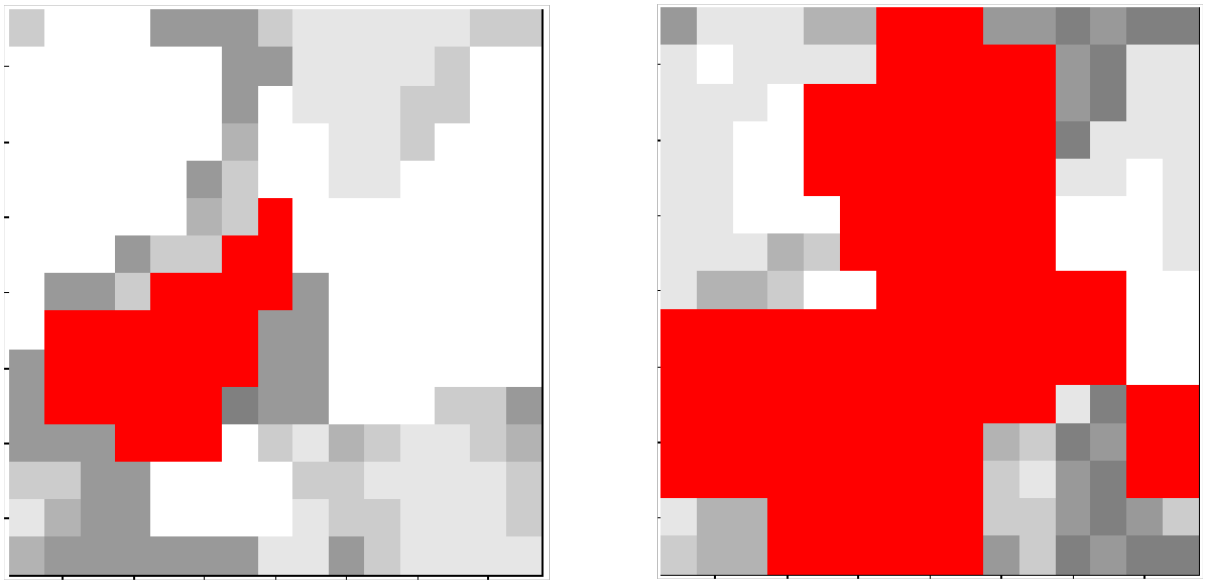

Figure 10: *Visualization of two randomly chosen fire events. The simulated area is nine hectare. The grey level indicates the amount of standing biomass. The red colour shows the fire spread.*

- **fire tolerance of trees:** According to the fire tolerance of a tree species, not every tree is burning and dying in the fire area. The probability for tree burning depends on fire tolerance of the species, on the stem diameter (D [cm]) as a proxy of tree age and on the fire severity [Busing and Solomon, 2006]. We distinguish between four fire tolerance levels for tree species. Tree species of level 1 are dying in a fire, independent of stem diameter or fire severity. Tree species with a fire tolerance up to level 4 have an increasing fire-resistance. The burning probability for every tree is calculated as follows depending on the fire tolerance of the tree species [Busing and Solomon, 2006]:

$$\begin{aligned} P_{F1} &= 1 \\ P_{F2} &= e^{((-(1-s_{fire})\cdot 0.00202)-0.00053)\cdot D} \\ P_{F3} &= e^{((-(1-s_{fire})\cdot 0.02745)-0.00255)\cdot D} \\ P_{F4} &= e^{-0.00053\cdot D} - 0.5 - (1-s_{fire})\cdot 0.5 \end{aligned}$$

where s_{fire} (value between 0-1) is an indicator for the severity and the type of the fire (Fig. 11) and D is the stem diameter.

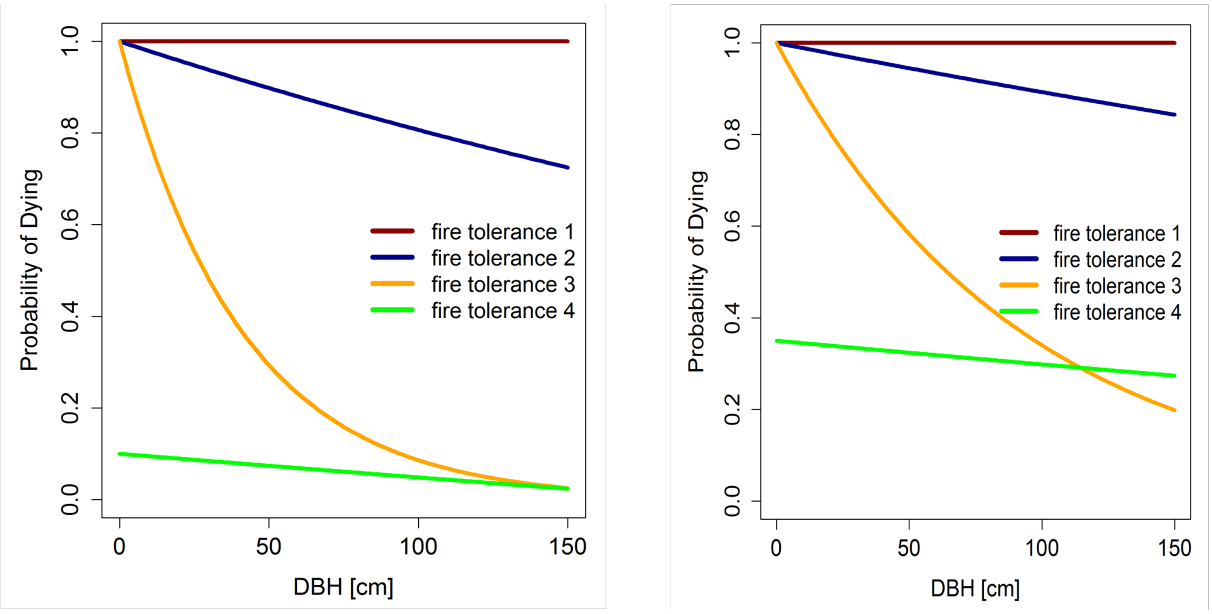

Figure 11: *Probability for tree dying after a fire event depending on stem diameter (D) and fire tolerance group. Left: probability of dying after a weak fire event (s_{fire}=0.2). Right: probability of dying after a strong fire event (s_{fire}=0.7).*

H.2 Landslides

In montane forests shallow landslides can constitute a recurring natural disturbance. Disturbance by landslides differs from disturbances by falling trees or logging in the sense that all vegetation, as well as upper soil layers and seed bank are removed from the disturbed patch. Forest regeneration on landslide surfaces therefore underlies particular environmental conditions. For instance, solar radiation on recent landslide sites is high and nutrient levels of landslide soils are low [Wilcke et al., 2003]. Due to this changed environmental conditions, establishment rates of trees as well as tree mortality and tree growth rates might deviate from the basic type-specific rates.

To study potential effects of landslide disturbances on the forest carbon cycle and species composition, we implemented landslides as a particular type of disturbance into the FORMIND 3.0 model. External inputs to the landslide module are the landslide frequency per hectare and year (*slidefreq*) and the distribution of landslide sizes. Landslide disturbance is implemented on the patch level, i.e. the smallest possible landslide has the size of one patch A_{patch} (i.e. 20 m x 20 m) and the biggest landslides considered are for example 25 patches (1 hectare).

We implemented landslides in the following way: for each hectare and in every year a

randomly drawn number determines whether a landslide occurs (probability f_{land}). Since the annual frequency on a per hectare basis will usually be small, we do not account for multiple landslides on one hectare in the same year. The size of the landslide is drawn from a size distribution (s) of landslides, rounded for the patch size A_{patch}. The starting location of the landslide is a random patch and the directionality of landslides is always the same. Neighbouring patches of the starting location are affected until the slide reaches the predetermined size.

All trees in landslide affected patches die and are removed from the patch. Since recruiting trees in FORMIND 3.0 have a stem diameter of D_{min} [cm] at breast height, there is a time lag (t_{lag}) between the landslide event and the occurrence of the first trees on the slide surface. Based on the potential growth of trees this time lag can be estimated for the different tree types. Forest recovery then proceeds according to one of the following scenarios: undisturbed regrowth, reduced growth, reduced recruitment, increased mortality. For the justification of these scenarios, see [Dislich and Huth, 2012]

- **Undisturbed regrowth:** All type-specific parameters stay unchanged. This situation considers increased light levels after the landslide disturbance but neglects additional environmental changes.

All other scenarios describe a temporal change in type-specific traits. The underlying assumption is that the strongest change in traits occurs immediately after the landslide and traits come back to their normal level, as forest recovery proceeds after the disturbance. The parameter r_{land} represents the assumed change in tree species attributes after landslide occurrence.

- **Reduced growth:** FORMIND 3.0 calculates tree growth as biomass increment per year (ΔB, cf. section G.3). Assuming a simple linear relation between growth reduction and 'recovery status' of the disturbed site, which is expressed by the ratio of accumulated dead biomass (B_{dead}) to the minimum biomass in a mature patch (B_{mat}), the reduced biomass increment (ΔB_{red}) is calculated via:

$$\Delta B_{red}(B_{dead}) = \left(r_{land} \cdot \frac{B_{dead}}{B_{mat}} + (1 - r_{land}) \right) \cdot \Delta B. \tag{76}$$

- **Reduced recruitment:** The type-specific recruitment rate per hectare and year (N_{seed}, cf. Appendix D) might be changed due to landslide disturbances. Like in the reduced growth scenario, we assume a linear relationship between the amount of recruitment reduction and recovery status of the patch, now expressed by the ratio of established biomass in the recovering patch (B_{pat}) to the minimum biomass of a

mature patch (B_{mat}). Therefore the reduced recruitment rate (N_{red}) is calculated via:

$$N_{red}(B_{pat}) = \left(r_{land} \cdot \frac{B_{pat}}{B_{mat}} + (1 - r_{land}) \right) \cdot N_{seed} \tag{77}$$

- **Increased mortality:** The type-specific mortality rate (M) might change due to landslide disturbance (cf. Appendix E). Again, we assume a linear relationship between the increment in mortality rate and the recovery status of the patch, represented by the ratio of established biomass in the recovering patch (B_{pat}) to the minimum biomass of a mature patch (B_{mat}). Therefore the increased mortality rate (M_{inc}) is calculated as:

$$M_{inc}(B_{pat}) = \left(1 + \left(r_{land} - r_{land} \cdot \frac{B_{pat}}{B_{mat}} \right) \right) \cdot M. \tag{78}$$

The choice of the parameter r_{land} as well as the chosen functional relationship between changed attributes and recovery state of the successional forest is adapted according to site specific knowledge. Exemplary values for the parameters t_{lag}, r_{land} and f_{land} are shown in table 5 and 6. The slide side distribution is given in 7

Table 5: *Exemplary values for the time lag parameter t_{lag} [Dislich and Huth, 2012].*

Type	t_{lag}
pioneer species	3
mid-successional species	5
climax species	12

Table 6: *Exemplary values for the parameters r_{land} and f_{land} [Dislich and Huth, 2012].*

Parameter	Value
r_{land}	0.9, 0.5
f_{land}	0.02

Table 7: *Exemplary slide size distribution s [Dislich and Huth, 2012].*

Landslide size $[m^2]$	Frequency
400	0.30
800	0.26
1200	0.16
1600	0.09
2000	0.08
2400	0.03
2800	0.03
3200	0.01
3600	0.03
4000	0.005
4400	0.005
≥ 4800	0

Appendix I Carbon cycle

The calculation of the carbon cycle in FORMIND 3.0 uses a simple compartment approach consisting of the following explicit carbon stocks:

- living forest stock, which equals the amount of carbon of alive trees
- deadwood stock S_{dead}, which equals the amount of carbon of dead trees
- slow decomposing soil stock S_{slow}, which accounts for the slow decomposing share of carbon in the deadwood stock
- fast decomposing soil stock S_{fast}, which accounts for the fast decomposing share of carbon in the deadwood stock

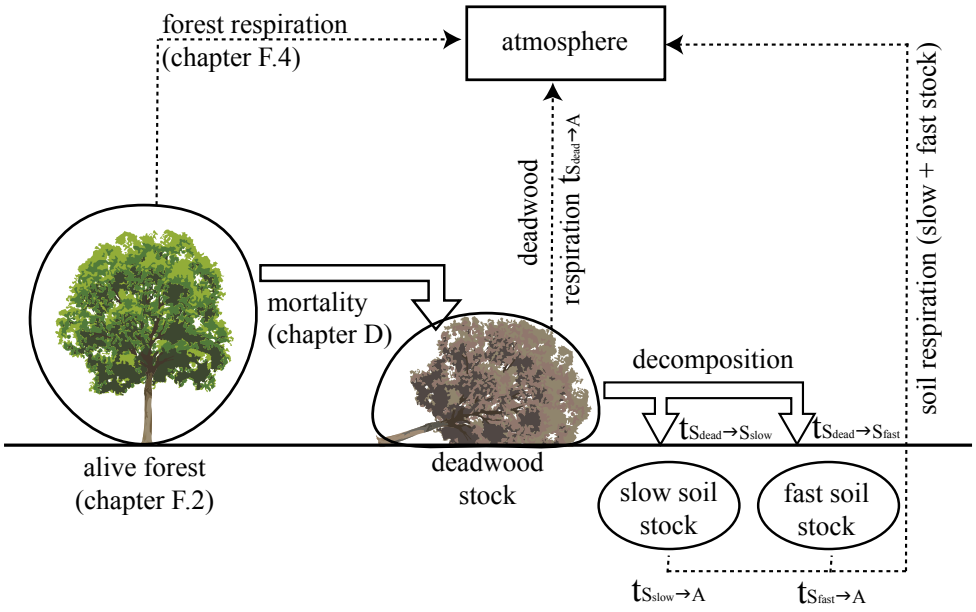

Figure 12: *Schematic visualization of the carbon cycle in FORMIND 3.0 . Circles represent explicit carbon stocks and the rectangle indicates the atmosphere. Dotted arrows show carbon released to the atmosphere from the respective stock and block arrows show carbon transitions between the respective explicit carbon stocks.*

The dynamics of the living forest stock (i.e. carbon storage in form of growth and carbon releases as respiration) are described earlier in Appendix G. The dynamics of the remaining stocks is described by a set of differential equations:

$$\begin{aligned}
\frac{\mathrm{d}S_{dead}}{\mathrm{d}t} &= S_{mort} - (t_{S_{dead}\to A} + t_{S_{dead}\to S_{slow}} + t_{S_{dead}\to S_{fast}}) \cdot S_{dead} \\
\frac{\mathrm{d}S_{slow}}{\mathrm{d}t} &= t_{S_{dead}\to S_{slow}} \cdot S_{dead} - t_{S_{slow}\to A} \cdot S_{slow} \\
\frac{\mathrm{d}S_{fast}}{\mathrm{d}t} &= t_{S_{dead}\to S_{fast}} \cdot S_{dead} - t_{S_{fast}\to A} \cdot S_{fast}
\end{aligned}$$

where the parameters $t_{S_{dead}\to A}$, $t_{S_{slow}\to A}$ and $t_{S_{fast}\to A}$ denote transition rates in $[1/\mathrm{yr}]$ of released carbon from the respective soil stocks to the atmosphere. The parameter $t_{S_{dead}\to S_{slow}}$ and $t_{S_{dead}\to S_{fast}}$ represent in turn decomposition rates of deadwood material in $[1/\mathrm{yr}]$. The variable S_{mort} $[t_C/\mathrm{ha}]$ represents the carbon of all trees dying within the current time step (see Appendix E).

I.1 Determining the transition rates

The transition rates depend on how fast microorganisms can decompose the fallen litter or dead trees. For describing the decomposition rates, we use an approach presented earlier by Sato et al. [2007]. The annual decomposition rate $t_{S_{dead}\to}$ for the deadwood stock is calculated as follows:

$$t_{S_{dead}\to} = \min\left(1.0, \frac{10^{-1.4553+0.0014175\cdot AET}}{12}\right), \tag{79}$$

where AET is considered as the actual evapotranspiration in the previous year in mm. The variable AET is calculated by the sum of interception IN and transpiration TR (cf. section F.2).

The annual decomposition rate $t_{S_{dead}\to}$ is modelled as the sum of all transitions rates of the deadwood pool S_{dead}:

$$t_{S_{dead}\to} = t_{S_{dead}\to A} + t_{S_{dead}\to S_{slow}} + t_{S_{dead}\to S_{fast}} \tag{80}$$

According to [Sato et al., 2007] 70 % of the carbon of decomposing deadwood biomass (i.e. litter) is directly released to the atmosphere, while the remaining 30 % are transferred to the slow and fast decomposing soil stocks. In detail, 98.5 % of the remaining carbon is transferred to the fast soil stock and 1.5 % to the slow soil stock. We then calculate the

specific transition rates as follows:

$$\begin{aligned} t_{S_{dead}\to A} &= 0.7 \cdot t_{S_{dead}\to} \\ t_{S_{dead}\to S_{slow}} &= 0.015 \cdot 0.3 \cdot t_{S_{dead}\to} \\ t_{S_{dead}\to S_{fast}} &= 0.985 \cdot 0.3 \cdot t_{S_{dead}\to} \end{aligned}$$

I.2 The Net Ecosystem Exchange (NEE)

The NEE is the carbon net flux of the forest. We define the NEE [$^{tC}/_{\text{ha yr}}$] as follows:

$$NEE = C_{GPP} - C_R - t_{S_{dead}\to A} \cdot S_{dead} - t_{S_{slow}\to A} \cdot S_{slow} - t_{S_{fast}\to A} \cdot S_{fast}, \tag{81}$$

where S_{dead} [$^{tC}/_{\text{ha}}$] denotes the deadwood carbon pool, S_{slow} [$^{tC}/_{\text{ha}}$] and S_{fast} [$^{tC}/_{\text{ha}}$] the soil carbon stock (i.e. slow and fast decomposing), $t_{x\to A}$ [$^{1}/_{\text{yr}}$] the corresponding transition rates of released carbon from the respective stock x resulting from the microbiological respiration (cf. section Appendix I) and C_{GPP} [$^{tC}/_{\text{ha yr}}$] is the carbon captured in the gross primary productivity of the living forest (cf. G.2), C_R [$^{tC}/_{\text{ha yr}}$] is the carbon released by the total respiration of the living forest (i.e. for maintenance and growth). We also assume here that 1 g organic dry matter contains 44 % carbon, which results in:

$$\begin{aligned} C_{GPP} &= 0.44 \cdot \sum_{all\ trees} GPP \\ C_R &= 0.44 \cdot \sum_{all\ trees} (R_m + R_g \cdot (GPP - R_m)). \end{aligned}$$

If the NEE is positive (i.e. $NEE > 0$), the forest is considered to be a carbon sink. If the NEE is negative (i.e. $NEE < 0$), the forest is considered to be a carbon source.

Appendix J Logging

Commercial trees are logged on selected areas. Trees with specific attributes are removed from the forest plot. At the same time, surrounding trees are damaged based on the chosen logging strategy, logging intensity, logging cycle, cutting limits and resulting damage [Huth and Ditzer, 2001; Huth et al., 2005].

J.1 Logging strategy

The two logging strategies L_S that are provided in FORMIND, arise from different commercial and economical interests. The two strategies differ in the falling direction of a logged tree:
The reduced impact logging (RIL) takes into account a substantial planning of the logging scenario. This scenario is implemented into FORMIND by defining the falling direction of a tree towards the biggest gap. Thereby, the falling tree causes a reduced amount of damage to surrounding trees.
The conventional logging (CON) takes into account the usage of heavy machinery, unskilled workers and low to no planing strategies. This is implemented into FORMIND by a random falling direction of logged trees. The random direction causes the possibility of higher damage to surrounding trees.

J.2 Logging intensity

The logging intensity is defined by the minimum number of trees harvested within the forest plot L_{Nmin} [-] and the maximum number of trees L_{Nmax} [-].

J.3 Logging cycle

The first logging scenario is defined as L_{start} [y]. The logging cycle is the time between logging events L_C [y].

J.4 cutting limit

Commercial trees are are only logged if their dbh exceed a minimum dbh L_Dmin.

J.5 logging intensity

Logging intensity is defined as the number of remaining commercial trees in the forest after the logging event L_{remain}.

J.6 damage

The induced damage to surrounding trees depends on the dbh of the logged tree - bigger trees cause more damage to surrounding trees than smaller trees. Therefore, a percental damange L_dam is defined for four different diameter classes L_dc.

Abbreviations

Symbol	Description
ODM	Organic dry matter
CO_2	Carbon dioxide
C	Carbon
H_2O	Water
sin	Sinus function
cos	Cosinus function
$\lfloor\rfloor$	Round down
e	Exponential function
ln	Logarithm function
cf.	see
e.g.	exempli gratia (for example)
i.e.	id est (that is)
Fig.	Figure
Tab.	Table

References

Botta, A., Viovy, N., Ciais, P., Friedlingstein, P., Monfray, P., 2000. A global prognostic scheme of leaf onset using satellite data. Global Change Biology 6, 709–725.

Busing, R.T., Solomon, A.M., 2006. Modeling the effects of fire frequency and severity on forests in the northwestern United States. Scientific Investigations Report 2006-5061, US Geological Survey.

Dislich, C., Günter, S.and Homeier, J., Schröder, B., Huth, A., 2009. Simulating forest dynamics of a tropical montane forest in south ecuador. Erdkunde 63, 347–364.

Dislich, C., Huth, A., 2012. Modelling the impact of shallow landslides on forest structure in tropical montane forests. Ecological Modelling 239, 40–53.

Fischer, R., 2010. Modellierung des Wachstums von Regenwäldern. Untersuchung der Auswirkungen von Trockenstress und Holznutzung auf den tropischen Regenwald am Beispiel des RNI Betampona (Madagaskar). Master's thesis. HTWK Leipzig.

Gardner, R.H., Romme, W.H., Turner, M.G., 1999. Predicting forest fire effects at landscape scales, in: Mladenoff, D.J., Baker, W.L. (Eds.), Spatial Modeling of Forest Landscape Change: Approaches and Applications., Cambridge University Press, Cambridge. pp. 163–185.

Granier, A., BrÃ©da, N., Biron, P., Villette, S., 1999. A lumped water balance model to evaluate duration and intensity of drought constraints in forest stands. Ecological Modelling 116, 269–283.

Green, D.G., 1989. Simulated effects of fire, dispersal and spatial pattern on competition within forest mosaics. Vegetatio 82, 139–153.

Gutiérrez, A.G., Huth, A., 2012. Successional stages of primary temperate rainforests of chiloé island, chile. Perspectives in Plant Ecology, Evolution and Systematics 14, 243–256.

Haxeltine, A., Prentice, C.I., 1996. A general model for the light-use efficiency of primary production. functional ecology 10, 551–561.

Huth, A., Ditzer, T., 2001. Long-term impacts of logging in a tropical rain forest - a simulation study. Forest Ecology and Management 142, 33 – 51.

Huth, A., Drechsler, M., Koehler, P., 2005. Using multicriteria decision analysis and a forest growth model to assess impacts of tree harvesting in dipterocarp lowland rain forests. Forest Ecology and Management 207, 215 – 232. Decision Support in Multi

Purpose Forestry Decision Support in Multi Purpose Forestry Selected papers from the symposium on Development and Application of Decision Support Tools in Multiple Purpose Forest Management.

Keane, R.E., Cary, G.J., Davies, I.D., Flannigan, M.D., Gardner, R.H., Lavorel, S., Lenihan, J.M., Li, C., Rupp, T.S., 2004. A classification of landscape fire succession models: spatial simulations of fire and vegetation dynamics. Ecological Modelling 179, 3–27.

Kumagai, T., Katul, G.G., Saitoh, T.M., Sato, Y., Manfroi, O.J., Morooka, T., Ichie, T., Kuraji, K., Suzuki, M., Porporato, A., 2004. Water cycling in a bornean tropical rain forest under current and projected precipitation scenarios. Water Resour. Res. 40, W01104–.

Lambers, H., Chapin III, F., Pons, T., 2008. Plant physiological ecology. Springer.

Larcher, W., 2001. Ökophysiologie der Pflanzen. Leben, Leistung und Stressbewältigung der Pflanzen in ihrer Umwelt. UTB für Wissenschaft, Verlag Eugen Ulmer Stuttgart.

Liang, X., Lettennmaier, D., Wood, E., Burges, S.J., 1994. A simple hydrologically based model of land surface water and energy fluxes for general circulation models. Journal of Geophysical Research 99, 14415–14428.

Monsi, M., Saeki, T., 1953. Uber den lichtfaktor in den pflanzengesellschaften und seine bedeutung fur die stoffproduktion. Jpn. J. Bot 17, 22–52.

Pfeiffer, M., Spessa, A., Kaplan, J.O., 2013. A model for global biomass burning in preindustrial time: Lpj-lmfire (v1.0). Geoscientific Model Development 6, 643–685.

Prentice, C.I., Sykes, M.T., Cramer, W., 1993. A simulation model for the transient effects of climate change on forest landscapes. Ecological Modelling 65, 51–70.

Sato, H., Itoh, A., Kohyama, T., 2007. Seib-dgvm: A new dynamic global vegetation model using a spatially explicit individual-based approach. Ecological Modelling 200, 279–307.

Thonicke, K., Venevsky, S., Sitch, S., Cramer, W., 2001. The role of fire disturbance for global vegetation dynamics: coupling fire into a dynamic global vegetation model. Global Ecology and Biogeography 10, 661–677.

Thornley, J.H.M., Johnson, I.R., 1990. Plant and crop modelling: a mathematical approach to plant and crop physiology. Oxford University Press.

Wilcke, W., Valladarez, H., Stoyan, R., Yasin, S., Valarezo, C., Zech, W., 2003. Soil properties on a chronosequence of landslides in montane rain forest, ecuador. CATENA 53, 79–95.